50th AIAA Aerospace Sciences Meeting including the New Horizons Forum and Aerospace Exposition
09 - 12 January 2012, Nashville, Tennessee
AIAA 2012-1167

Time-Domain Analysis of Subsonic Jet Noise

M. Kearney-Fischer[1], A. Sinha[2] and M. Samimy[3]
Gas Dynamics and Turbulence Laboratory
Aeronautical and Astronautical Research Laboratories
Department of Mechanical and Aerospace Engineering, the Ohio State University
2300 West Case Road
Columbus, Ohio 43235-7531USA

Following on previous works showing that jet noise has significant intermittent aspects, the present work assumes that these intermittent events are the dominant feature of jet noise. A definition and method of detection for intermittent noise events is devised and implemented. Using a large experimental database of acoustically subsonic jets with different acoustic Mach numbers (M_a = 0.5 – 0.9), diameters (D = 2.54, 5.08, & 7.62 cm), and exit temperature ratios (ETR = 0.84 – 2.70), these events are extracted from the noise signals measured in the anechoic chamber of the NASA Glenn AeroAcoustic Propulsion Laboratory. It is shown that a signal containing only these events retains all of the important aspects of the acoustic spectrum for jet noise radiating to shallow angles relative to the jet downstream axis, validating the assumption that intermittent events are the essential feature of low angle jet noise. The characteristics of these noise events are analyzed showing that these events can be statistically described in terms of three parameters (the variance of the original signal, the mean width of the events, and the mean time between events) and two universal statistical distribution curves. The variation of these parameters with radiation direction, diameter, velocity, and temperature are discussed. A simple model for this kind of signal is formulated and used to derive a relationship between the characteristics of the noise events and the fluctuations in the integrated noise source volume.

Nomenclature

A_i	=	i^{th} event amplitude (Pa)
a_∞	=	ambient speed of sound (m/s)
D	=	jet exit diameter (cm)
ETR	=	jet Exit Temperature Ratio
$G(x;\ell,\xi)$	=	gamma distribution
He	=	Helmholtz number (f D/a_∞)
ℓ	=	shape parameter of the gamma distribution
M_a	=	jet acoustic Mach number (U_j/a_∞)
$N(x;\sigma,\mu)$	=	normal distribution
p	=	far-field acoustic pressure (Pa)
p_{RMS}	=	root mean square pressure (Pa)
St_D	=	Strouhal number (f D/U)
T_i	=	i^{th} event temporal coordinate (s)
U_j	=	jet exit velocity (m/s)
$\underline{x}$	=	far-field observer coordinates (m)
$\underline{y}$	=	source-field coordinates (m)
α	=	model event width parameter (μs)
$\overline{\Delta T}$	=	mean event intermittence (msec)
$\overline{\delta t}$	=	mean event width (μs)
δt_i	=	i^{th} event width (μs)
σ	=	standard deviation parameter of normal distribution (Pa)
τ_∞	=	inverse Helmholtz number
τ_j	=	inverse Strouhal number

[1] Postdoctoral Research Associate. AIAA member.
[2] Ph.D. Student; Currently Postdoctoral Research Associate at CalTech. AIAA member.
[3] Nordholt Professor of Mechanical and Aerospace Engineering, AIAA Fellow, Corresponding author: samimy.1@osu.edu

ϕ = jet polar angle relative to downstream axis (degrees)
ξ = scale parameter of the gamma distribution (μs)
Ψ_{ij} = integrated noise source tensor (kg m^2 s^{-2})

I. Introduction

JET noise is a problem that has plagued the use of jet engines since their inception. Despite more than six decades of research since the seminal work of Lighthill [1], a clear picture of jet noise sources has not yet been emerged [2]. Part of the problem is the sheer number of parameters that can be varied in a jet that have been shown to impact jet noise production (e.g. temperature, pressure, density, hydrodynamic Mach number, acoustic Mach number, nozzle geometry, exit boundary layer turbulence, etc.). Many of these parameters are interrelated and no unified standard exists for reducing them to the minimum set of independent parameters – this leads to additional confusion about overlapping experimental regimes. While there have been advances in empirically based models [e.g. 3, 4] and theoretical analysis [e.g. 5] of jet noise, the essential features of jet noise are still debated. Without a complete description of the essential features of jet noise, understanding of their sources is clearly impeded.

Through six decades of research, there have been two dominant methods of experimental data analysis in jet aeroacoustics: 1) Fourier spectrum analysis and 2) correlation analysis. Spectral analysis is the fundamental tool used by the aeroacoustics community, and for good reason. These two tools provide researchers with a wealth of information and insight, but with certain restrictions. Spectral analysis discards temporal information making it impossible to link particular aspects of the frequency domain back to segments of the signal in time. Correlation analysis provides links between two signals in time, but only if their trends are sufficiently similar – it can indicate how similar the trends of two signals are and how the similarity is displaced in time.

The problem with the reliance on these two tools, particularly spectral analysis, is that they are likely to overlook some of the fundamental aspects of jet noise. Relatively recently, some researchers have started utilizing tools like wavelet transforms to obtain a more complete picture of the noise signal. The basic theme of these works is the supposition that acoustically subsonic jet noise (at least in the radiation to low angles) is made up of intermittent bursts as opposed to continuous variations. Understanding this kind of signal requires a different analysis methodology than has been prevalent in the literature. In a previous work from the Gas Dynamics and Turbulence Laboratory (GDTL) of the Ohio State University, Hileman *et al.* [6] showed that, if the amplitude of intermittent bursts (in this context defined as portions of the signal that exceeded twice the root mean square pressure, 2 p_{RMS}) were reduced by 50%, the peak region of the spectrum was reduced by about 4 dB. Hileman *et al.* used the assumption that the bursts are a significant constituent of the noise signal, but not necessarily the primary feature. The purpose of the present paper is to take this previous assumption to its extreme limit: assume that these bursts (hereafter referred to as noise "events") are the dominant feature of jet noise. The paper is divided as follows.

- A noise event as well as a method of its identification and extraction is defined and discussed.
- The spectrum of the event-only signal is computed and compared to the total signal.
- Statistical analysis of these events is performed for an extensive experimental data set to reveal what these events can say about the nature of jet noise.
- The implications of the statistical analysis on jet noise sources are discussed.

II. Background

Fourier spectrum analysis (known as Fourier analysis, spectral analysis, frequency analysis, and many other names in the literature) is a powerful tool used throughout the scientific world for signal analysis of all kinds. This approach has contributed to many of the currently understood aspects of jet noise including, but not limited to: directivity, scaling with size and velocity, and identifying different types of noise sources. Consequently, this tool is a staple of the aeroacoustics community and a benchmark for any new theory or analysis technique. One example utilizing spectral analysis is Viswanathan's work on scaling [4] that incorporates temperature and directivity effects into an empirical model for noise scaling. Another example of the power of spectral analysis is Tam's development of the two noise-source model [3, 7] which shows that the mixing noise in jets can be described by two types of source spectra that are superposed with different weights at different polar angles.

Correlation analysis is another powerful tool that has contributed to many of the same areas of understanding of jet noise as spectral analysis [e.g. 8-11]. Studies utilizing this tool are looking for relationships between different variables (e.g. velocity and density) or the same variables but at different regions of interest in a flow (e.g. near-field to far-field or flow-field to far-field). Typically, signals from different points in space are correlated to look at the relationships between those locations in terms of propagation or directivity. Many of these studies use correlation

analysis to locate noise sources in space and/or time in an attempt to link the result (i.e. acoustic radiation) back to the cause (i.e. the turbulent dynamics that produce the noise).

The papers cited above are but a few examples of the enormous body of work that has been generated in the decades of research on jet noise. These examples were chosen simply to provide concrete instances of different utilizations of these tools. For many hundreds more examples of works utilizing these tools in the pursuit of understanding jet noise, the reader is referred to any of the several review papers that have been written on the subject [2, 12-15].

For the details of the present understanding of jet noise, the reader should refer to the cited review papers, but the general summary is as follows. The noise from a turbulent jet consists of several major components. It is well established that there exist flow structures (vortices) ranging in size from dissipation-scale to the order of the nominal exit dimension of the jet nozzle (i.e. large-scale structures). It is generally accepted that jet noise is produced by the interaction, as well as disintegration of these structures. Beyond this point, the description of noise production processes gets quite complicated. In subsonic jets, the interaction and disintegration of flow structures produce what is known as mixing noise. A supersonic jet could also include screech and broad-band shock-associated noise. Depending on the velocity of the jet and the acoustic properties of the fluid into which the jet is exhausting, there is yet another noise component known as Mach wave radiation. Some of these noise production mechanisms are fairly well understood while others are not; the interdependence of the various mechanisms is not easily identified. While the basic governing dynamics behind screech and Mach wave radiation have been known for decades, the basic production mechanisms for mixing noise remain elusive. Theoretical approaches to the problem have provided insights, but an elegant description of a source and its relationship to the noise produced has not been obtained. Theoretical analyses, beginning with the pioneering work of Lighthill, struggle to untangle the non-linear nature of the governing equations into a form that clearly identifies a source.

II.A. Vortex Sound

As already stated, it is generally believed that the dynamics of vortices present in the flow are responsible for sound production. A more specific flow-noise relation is the belief that the dynamics of large vortices (i.e. large-scale structures) are responsible for the dominant sound radiated to low angles relative to the jet downstream axis. It has been speculated that dynamically significant events, as opposed to the mere existence of the structures, (e.g. the collision/interaction of two vortices or breakup of a vortex) are the mechanism that produces the noise radiated to the low angles. Thus the research on vortex sound has a close relationship to research on jet noise. Vortex sound theory, originally developed by Powell [16], and refined by Möhring [17] and others, was first experimentally tested by Kambe *et al.* [18-20]. The experimental work of Kambe *et al.* shows that the theory does a reasonably good job of predicting the noise generated by the head-on collision of two vortex rings. The sound pressure signal p produced by these collisions appears as a primary peak accompanied by two lower amplitude side-lobes. Their work has also shown that these collisions produce a primarily quadrupole sound field whose amplitude scales as

$$p \propto \frac{U^4}{r}, \tag{2.1}$$

where U is the collision speed of the vortices and r is the radial distance to the observation point. In terms of intensity, these collision noise events follow the same U^8 scaling as derived by Lighthill for jet noise. Additionally, they revealed that these events have a non-dimensional characteristic lifetime that scales as R_o/U, where R_o is the initial radius of the vortex ring.

Another important example of experimental work on vortex sound is the research of Schram *et al.* [21, 22]. This work focuses on the sound generated by ring vortex pairing events in low-speed jets ($U_j \approx 5$ & 34 m/s). Using a combination of excitation, axisymmetric geometry assumptions, and PIV, they were able to calculate the integrated source term from the velocity field and, therefore, calculate the acoustic pressure fluctuation produced by the pairing. By examining two different jet velocities, they observed that the structure of the acoustic pulse became more complex with increasing velocity. In the 5 m/s jet, vortex pairing produced an acoustic pulse that was essentially a single prominent peak with weak side-lobes of opposite sign. In the 34 m/s jet, pairing resulted in an acoustic pulse with two prominent peaks, one positive and one negative, with an additional weaker lobe on each side of the primary pulse.

Although much of the experimental work has focused solely on the head-on collision of two vortex rings, the sound produced by this well-studied type of vortex collision is a passable model for the kinds of sound events created by various unsteady vortex processes. There have also been theoretical and simulation-based works looking

at a wider variety of vortex phenomena and their sound production [e.g. 23-25]. This is an ongoing and active area of research and its precise relevance to jet noise is still unclear.

If it is accepted, however, that dynamics of large-scale structures such as interaction and disintegration (or vortex collision/decay) are the dominant mechanism of sound production in a jet, then the theory of vortex sound dictates several aspects of the acoustic signal. The most important aspect is intermittence. In this model, the sound source is not continuous and this means that spectral analysis is likely masking important characteristics. Additionally, while the rate of vortex creation in the jet can be thought of as being approximately periodic (at the jet column natural Strouhal number of $St_D \approx 0.3$), the timing of vortex collision/decay processes would be only loosely dictated by the creation timing. This is another area where spectral analysis may have trouble since by design it has a preference for periodic signals. The last area of relevance is the shape of the radiated sound wave and its relationship to the sources; specifically the implications for wave-packet models of sound sources. A good discussion of the history and development of wave-packet models is given by Obrist [26]. Almost all existing wave-packet models are based on simple travelling waves that produce far-field sound signals that are highly periodic and whose characteristic lifetimes (the reader can think of time between zero crossings as a metric of the lifetime for the present purposes) are on the same order as the period of the travelling source. These source periods are often modeled as being driven by the large-scale structure periodicity (i.e. dictated by $St_D \approx 0.3$). Within the framework of vortex sound describing jet noise, the characteristic shape and lifetime of the noise events would have little relation to the period between large-scale structures and a completely new source model would be needed.

II.B. Temporally Localized Signal Analysis

Fourier analysis utilizes oscillating signals with infinite extent and describes the examined signal in terms of those oscillations. Therefore it is not particularly useful for characterizing localized events.

Even without reference to the preceding discussion on the efficacy of vortex sound as framework for understanding jet noise, a few researchers have chosen to look at the acoustic far-field with the assumption that at least some of the sources of noise are intermittent [e.g. 6, 27-34]. A common theme that unifies these works is the use of wavelet analysis – the underlying principle of which is that the signals under examination cannot be adequately described by a set of periodic waves. This assumption of intermittence has produced some interesting results.

In the case of the previous works at GDTL [6, 27], the assumption of intermittence provides a basis for a source localization method. A wavelet transform of the far-field signal showed that there were spikes in the signal. Based on this observation, noise events were defined as spikes rising above a specified threshold in the time domain. The localization method used a microphone array, and the times of arrival at the various microphones of these spikes to locate the source of an event in space-time. As discussed in those works, the calculated region of noise sources agrees with other research indicating that the noise radiated at low angles (~30°) relative to the jet downstream axis comes from an area near the end of the potential core. Simultaneous flow-visualizations using a MHz-rate imaging system showed that these events are associated with dynamically significant behavior of the large-scale structures. It was also shown that when the amplitude of the events was artificially reduced via signal post-processing, the amplitude of the spectral peak could be reduced by several decibels. Guj *et al.* [32] used a similar kind of conditional averaging of the flow-field to determine that bursts of noise were related to dynamically significant fluctuations of the large-scale structures. They also called attention to the limitations of Fourier analysis to illuminate this kind of phenomenon.

Cavalieri *et al.* [29] look at the direct numerical simulations (DNS) of an uncontrolled and an optimally noise-controlled two-dimensional mixing layer of Wei and Freund [35]. They show that the optimally controlled case accomplishes noise reduction by suppressing certain intermittent peaks in the signal – highlighting the need to include intermittency in sound prediction schemes. Noise suppression in this simulation was related to preventing the merger of three vortices (a triple-merger) that was shown to produce a large spike in the acoustic signal. Cavalieri *et al.* [30] discuss a wave-packet model in which the envelope function varies in both space and time. This analysis, which follows the idea originally suggested by Kastner *et al.* [36], shows that a high amplitude event (i.e. a pressure spike) can be produced when the wave-packet is truncated by fluctuations in the envelope. Grassucci *et al.* [28] use a wavelet domain filter to separate near-field pressure fluctuations into intermittent and non-intermittent signals. They then relate the intermittent signal to velocity fluctuations in the jet using Linear Stochastic Estimation (LSE). While this work is preliminary, their initial results are promising. Kœnig *et al.* [31, 37, 38] have started using wavelet transforms and filtering in the wavelet domain to isolate these intermittent events for study. This analysis uses a 4^{th} order Paul wavelet to decompose the signals with a continuous wavelet transform. Results to date have mainly focused on the relationship of the resulting directivity patterns to wave-packet models for jet noise. One

important observation in Kœnig *et al.* [37] is that using Helmholtz number can achieve better spectral collapse for varying acoustic Mach number than Strouhal number scaling in unheated jets. This scaling with Helmholtz number has also been seen by other researchers [e.g. 39] and is further discussed in §VI. Low *et al.* [34] uses wavelet filtering and correlation on both near and far-field to determine how the near-field events are related to the far-field events. Their work is still preliminary, but warrants mentioning as a significant attempt to trace the intermittent aspects of jet noise back toward their sources.

These works show that jet noise does indeed contain intermittent events and that these events play a significant role in the overall acoustic picture of the jet. The results to date, however, are quite limited in their description of these intermittent events. Issues such as the importance of these events to the total signal spectra, many aspects of the nature of these events (lifetimes, frequency of occurrence, etc.), and exact relationship of these events to the flow-field dynamics remain to be determined.

III. Noise Event Definition and Signal Extraction

The hypothesis of this analysis is as follows.

> **Hypothesis:** *The primary noise sources in a mixing noise dominated jet (i.e. acoustically subsonic), at least those that radiate to shallow angles relative to the jet downstream axis, are intermittent "events" with periods of relative silence in between.*

Therefore, a post-processing routine that highlights these events while suppressing other signal components can shed light on the relevant dynamics of jet noise. While some of the previous work of other researchers lends support to this premise, only the work of Kœnig *et al.* [see 37 and others] has made the assertion that these events constitute the dominant mechanism of jet mixing noise. The validity of this premise will be investigated once the analysis process has been explained.

In the absence of a theoretical basis, this analysis requires an ad hoc definition of an event. In this analysis, an event is defined as a portion of the signal whose peak exceeds $\pm 1.5 p_{RMS}$ where the RMS pressure is a unique value for every microphone (dictated by its position in the acoustic field) and the jet operating condition. This definition is chosen because it is consistent with the previous work at GDTL [6, 27]. While the definition of Kœnig *et al.* [37] uses an arbitrary threshold in the wavelet domain, the current approach applies the thresholding in the time domain. The complementary nature of these two approaches is beneficial, primarily because it should be useful for comparison to the two results for both contrast and confirmation. Other multiples of p_{RMS} were explored and it was found that 1.5 was the largest threshold that sufficiently reproduced the important spectral characteristics (see §V). As one might expect, the distribution of amplitudes in a far-field noise signal—once normalized by p_{RMS} for that signal—is the unit normal distribution (this is demonstrated in §VI.A). The proportion of a signal contained within z standard deviations is given by

$$proportion(z) = \mathrm{erf}\left[z/\sqrt{2} \right], \tag{3.1}$$

where erf is the error function. Evaluated at $z = 1.5$, $proportion(1.5) = 0.866$ so this definition ignores about 87% of the signal time. It is important to take note of the fact that this threshold is unique for every signal. This selection criterion means that noise events are outliers with respect to the total signal in which they exist and this definition is self-consistent across any signal examined. A selection criterion based on a fixed threshold (either for the entire range of polar angles or based on a particular operating condition) would impose a definition that obviously would be incapable of accounting for scaling. Since these events might be expected to scale with properties like jet velocity and diameter, a definition that inherently scales is a superior choice. Another reason for this definition is that it is simple. Part of the motivation of this analysis is to see if the acoustic signals can be represented by a simplistic set of parameters.

A cartoon of the data extraction and fitting process for the basic types of encountered events is shown in Fig. 1. As discussed in more detail in §V, the events in the figure are fitted with a Mexican hat type wavelet. The wavelet reconstruction of each event is shown as a separate curve and the final events only waveform is also plotted. Information on the events is extracted as follows:

1. Any contiguous set of points that exceeds the threshold ($\pm 1.5 p_{RMS}$) is identified as an event – this identifies five regions in the cartoon (1, 2, 3, 4a, & 4b).
2. For every event i, the peak amplitude (A_i) and temporal location (T_i) are identified.
3. The width of an event (i.e. its extent in time – δt_i), defined as the width at half of the peak amplitude—i.e. the Full Width at Half Maximum (FWHM), is found by scanning outward in both directions from a given peak for the first occurrence of that criterion.

4. A check is performed to look for event overlap – events 4a and 4b in the cartoon. If the temporal extent of two or more peaks of the same sign overlaps, these events are merged into a single peak with the following properties.
    a. Width – Determined as the time between the left edge of the earliest peak and the right edge of the latest peak (time increasing from left to right) using the half-maximum criterion from the individual peaks.
    b. Peak Location – Determined as half way between the newly determined beginning and end of the merged peak.
    c. Peak Amplitude – the greatest amplitude in the merged event.

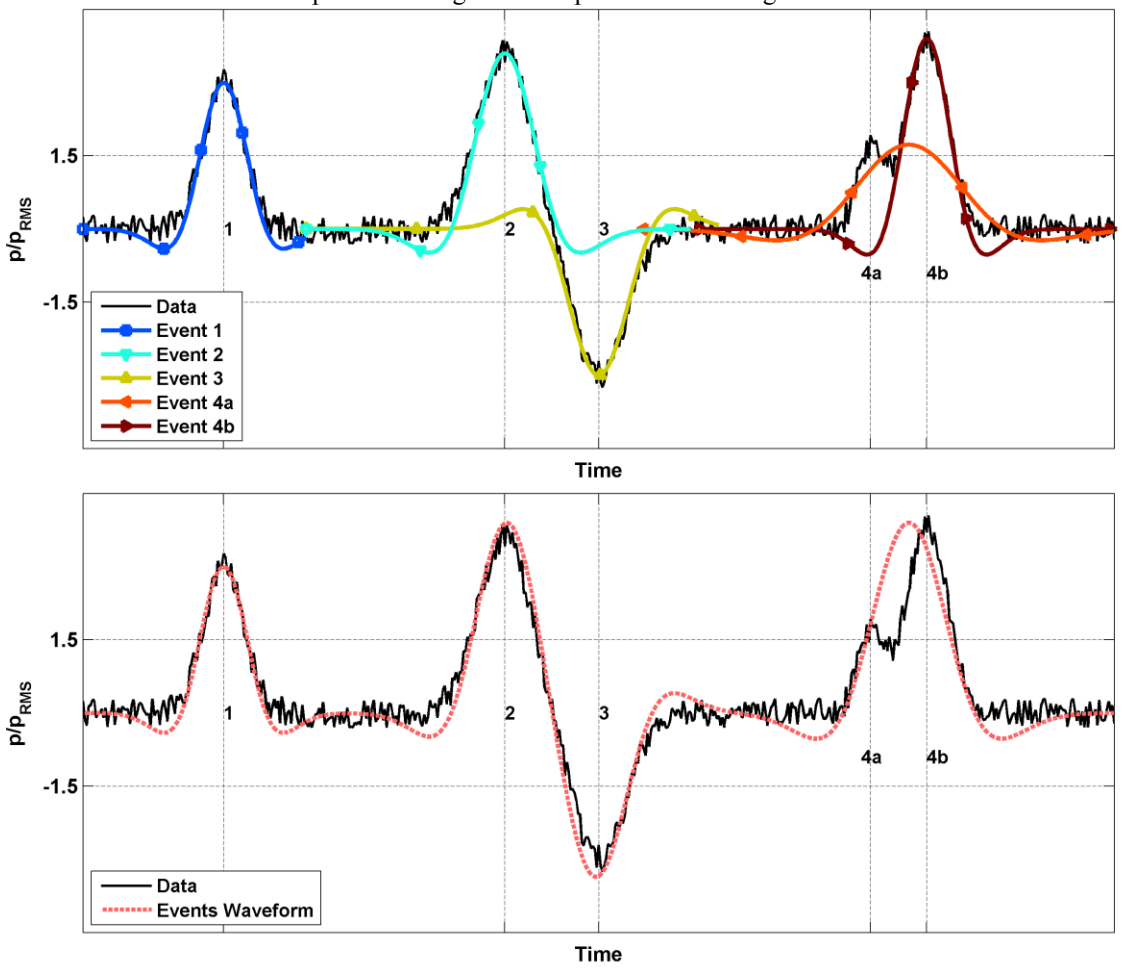

Fig. 1: Cartoon of data extraction process.

It should be noted that event location and width are determined to single sample accuracy of the discretely sampled acoustic signal and are not interpolated to a higher precision. One consequence of this data extraction method is that the minimum event width allowed is three samples. Any subsequent analysis of these quantities will also be quantized at single sample accuracy. With this information in hand, any number of analyses can be performed. In §VI these quantities are used to develop a statistical picture of the typical event characteristics.

IV. Experimental Database

The experimental database for this analysis is taken from the Small Hot Jet Acoustic Rig (SHJAR) at the NASA AeroAcoustic Propulsion Laboratory (AAPL). This database, taken from a large facility validation database study [40, 41], is designed to efficiently and effectively explore the various parameters that can affect subsonic jet noise. There are a total of 21 cases covering three jet diameters, five acoustic Mach numbers, and unheated as well as three elevated temperatures. All three of the nozzles in these experiments are axisymmetric. The exact values of these parameters are enumerated in Table 1. The "Case Number" will be used later in the paper to refer to the different

combinations of nozzle and operating conditions. Total Temperature Ratio (TTR) is the ratio of the jet stagnation temperature to the ambient temperature and the Exit Temperature Ratio (ETR) is the ratio the jet exit temperature to the ambient temperature. Unless stated otherwise, the Mach number referred to when discussing the data is the acoustic Mach number ($M_a = U_j/a_\infty$).

Table 1: Experimental operating conditions

D (cm)	TTR	M_a	ETR	Case Number
2.54	1.00	0.5, 0.6, 0.7, 0.8, 0.9	0.95, 0.93, 0.90, 0.87, 0.84	1-5
5.08	1.00	0.5, 0.6, 0.7, 0.8, 0.9	0.95, 0.93, 0.90, 0.87, 0.84	6-10
	1.81, 1.92	0.5, 0.9	1.76	16-17
	2.31, 2.43	0.5, 0.9	2.27	18-19
	2.75, 2.84	0.5, 0.9	2.70	20-21
7.62	1.00	0.5, 0.6, 0.7, 0.8, 0.9	0.95, 0.93, 0.90, 0.87, 0.84	11-15

The SHJAR is housed in a fully anechoic geodesic dome (60-foot, 18.3 m, radius) that uses 24 inch (61 cm) long fiberglass wedges to eliminate reflections at all frequencies above 200 Hz. Compressed air (up to 150 psia, 1.03 MPa) is routed through a hydrogen gas combustor, a muffler, settling chamber, and then through a reducer and nozzle where it is exhausted through a large door to the ambient environment. The combustor produces tones as well as broadband combustion noise that complicate data analysis because they are not fully eliminated by the muffler. The facility can support flow rates up to 6 lbm/s (2.72 kg/s) with stagnation temperatures up to 1300 °F (704 °C). This facility has 24 microphones on a constant radius arc ranging from 15° to 130° relative to the jet downstream axis spaced every 5°. The arc radius is 100 inches (2.54 m) from the nozzle exit for the 1" (2.54 cm) and 2" (5.08 cm) nozzles and 150 inches (3.81 m) for the 3" (7.62 cm) nozzle to ensure that microphones are in the acoustic far-field. All microphones are arranged for normal incidence on stands designed to minimize reflections. Data at this facility are acquired using Bruel & Kjaer model 4939 microphones and Nexus 2690 amplifiers connected using 100m cables. The output of the amplifiers are acquired at 200 kHz and low-pass filtered at 90 kHz by a DataMAX Instrumentation Recorder from RC Electronics Inc. About 8 seconds of data are acquired at each set point. Ambient conditions are monitored in real time to ensure that the properties like acoustic Mach number and ETR can be maintained. Many details such as the nozzle design and validation of the facility are available in [40, 41].

V. Spectral Analysis

The first order of business is to determine if the proposed definition of an event has any merit (i.e. does it capture the important aspects of the signal). Given that spectral analysis is the standard tool of research on jet noise, it would be useful to compare the spectrum of the original signal to one that contains only the events. One method to accomplish this kind of decomposition is filtering in the wavelet domain as already discussed in the context of the work of Kœnig *et al.* [31]. This approach is quite involved, but results in a decomposed signal containing events with intricate shapes. If, alternatively, the raw signal was simply truncated (i.e. $p(|p| < 1.5p_{RMS})$ were set to zero), it would introduce a lot of high frequency content from the sharp corners at the edges of an event. Given that the event locations, amplitudes, and widths are known, it is relatively easy to reconstruct an event decomposed signal with the appropriate choice of a model function. The model function chosen for this reconstruction is a Mexican hat type wavelet

$$\psi_i(t) = A_i\left(1-\frac{(t-T_i)^2}{\delta t_i^{\,2}\epsilon}\right)\exp\left[\frac{-(t-T_i)^2}{\delta t_i^{\,2}\epsilon}\right], \tag{5.1}$$

where A_i is the peak amplitude, δt_i is the event width (i.e. FWHM), T_i is the temporal location of the event peak, and ϵ is an empirical adjustment factor to skew the width of the wavelet based on the width as determined from the data. By trial and error, it was found that a correction of 10% was needed to adjust the wavelets to satisfactorily fit the data (i.e. $\delta t_{\text{wavelet}} = 0.9\ \delta t_i = \epsilon^{1/2}\ \delta t_i$). Therefore, $\epsilon = 0.81$ was set as a constant for all data processing. The cartoon in Fig. 1 demonstrates the fitting process. This model function was chosen because of its flexibility. If the true nature of a noise event is a single peak in isolation (event 1 in the cartoon), this function will probably fit it well unless it is highly asymmetric. If, however, the true nature of a noise event is more complex (i.e. involving multiple positive and negative swings such as the combined structure of events 2 and 3 in the cartoon), guessing an appropriate universal model function at this point is essentially impossible. Under the current definition, each positive and negative peak in a multiple swing event will be identified as a separate event and their parameters stored

independently. When the events-only signal is reconstructed, the different pieces will be modeled as independent instances of the Mexican hat wavelet. Since the Mexican hat wavelet is amenable to superposition (hence its use as a wavelet), it should do a good job of representing a more complex shape (see cartoon events 2 and 3). Once the reconstructed signal is calculated, it can be put through the same post-processing steps as the raw data for calculating the spectrum.

An example of the signal reconstruction is shown in Fig. 2 for three polar angles (ϕ = 30°, 90°, & 130°). The abscissa is a non-dimensionalized time, $\tau_j = t\ D/U_j = 1/St_D$ (inverse Strouhal number), where U_j is the jet exit velocity. The reconstruction is doing a good job, especially at the low angles, of reproducing the major aspects of the signal. At low angles, the time-domain is characterized by large slowly oscillating shapes. In contrast, the sideline and upstream angles are quite jittery (i.e. characterized by rapid oscillations on the order of the sampling resolution). The implications of these different characteristics are discussed in more detail using the statistical analysis in §VI.

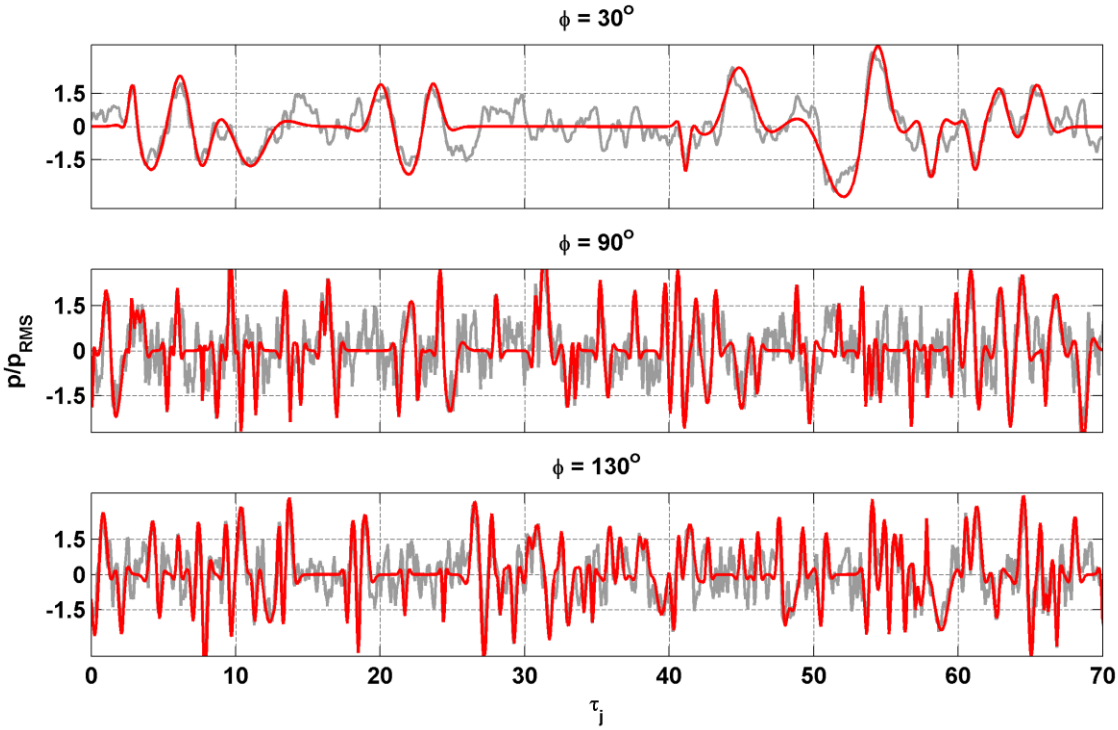

Fig. 2: Time-domain of a portion of data for D = 2.54 cm, TTR = 1.0, and M_a = 0.9 at three polar angles (ϕ = 30°, 90°, & 130°) showing the raw data (gray) and the reconstructed signal (red).

The Sound Pressure Level (SPL) spectra for the raw data and reconstructed data at two polar angles (ϕ = 30° & 90°) are shown in Fig. 3 for two disparate jets and operating conditions. It is clear that, especially in the case of 30°, the reconstructed signal is doing a very good job of reproducing the important features of the spectrum (i.e. the peak location and amplitude and the shape of the spectral peak). The decreased high frequency content is expected since the reconstruction ignores the high-frequency content of the signal except for that which is imposed by the width of events. There is also an increase in the low frequencies, probably due to the basic spectral behavior of the model function which requires all frequencies, below a characteristic frequency to represent the localized pulse. The higher angles (90° being the representative sample) are reasonably well reproduced, but the spectral amplitudes are slightly over-predicted. It is worth noting that no corrections have been applied to these spectra. In typical spectral analysis, a microphone free-field correction, distance scaling correction, and an atmospheric absorption correction are applied to the calculated spectrum. It was found that the frequency dependent corrections, which have significant effect only at high frequencies, do not meaningfully alter the characteristics of the signal relevant to this analysis. Additionally, since the definition and subsequent analysis are in terms of p_{RMS}, it is not necessary to scale the data to a uniform distance.

Some additional information can be gleaned at this point by looking at the energy of the reconstructed signal ($E_R = \langle (p - p_{mean})^2 \rangle$) compared to the original (E). The ratio of E_R/E is found to be essentially unity. Examining the various polar angles, it is found that this ratio has a range of 1±0.025. This unity or slightly over unity reconstruction

occurs because the smooth function used to model the events ends up adding some energy at low frequencies (as already discussed) which makes up for the energy eliminated from the high frequencies.

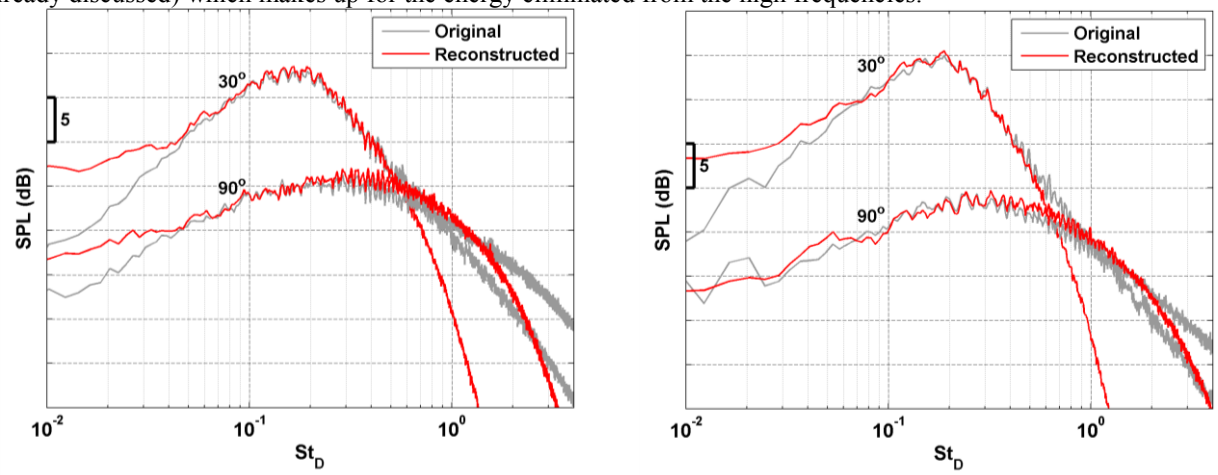

a) D = 2.54 cm, TTR = 1.00, M_a = 0.9 **b)** D = 5.08 cm, TTR = 2.84, M_a = 0.9

Fig. 3: Example spectra for signal reconstruction.

While there are many cases and polar angles that are not shown, these results are typical for all the cases studied. The low polar angles are well predicted by the event-only signal. The sideline and upstream angles are decently represented, but with the spectral amplitudes being a bit over-predicted. Without any additional analysis, these observations provide us some important insights.

1. This combination of event definition, data extraction, and signal reconstruction is capturing the vital aspects of jet noise using a simple set of equations with three parameters and a model function. It can therefore be concluded that acoustically subsonic jet noise (at least for the low polar angles) is indeed well described by a fundamentally intermittent signal populated by localized events.
2. The noise radiated to the sideline and upstream angles has a distinct nature that is detectable in this analysis. As will be further quantified in §VI, the educed noise events in these directions seem to have widths dictated by the sampling rate of the signal (i.e. the oscillations are too fast to be reasonably well resolved in the raw data). This kind of rapid oscillation can cause the determined event widths to be larger (typically by one sample) than the actual oscillation that they try to capture. These small amounts of added energy are likely the source of the over-predicted spectral amplitude since there are many events in the signal (in comparison to the shallow angles).
3. Based on the two preceding observations, it is concluded that the hypothesis is correct for low angles, but that sideline and upstream angles have a different nature. The exact nature of these signals will be quantified by further analysis in §VI.

VI. Statistical Analysis

Using the large number of events captured in a given data set for each polar angle (between 10,000 and 100,000 events depending on polar angle), it is possible to construct statistical distributions for the various quantities extracted from the data. The purpose of this section is to explore the nature of these extracted quantities through statistical analysis to determine how these quantities scale with jet diameter and operating conditions. This is accomplished by examining the distributions of the three parameters (amplitude, location in time, and width) and determining scaling quantities for these parameters. In most of this section, analysis will be focused on 30° and 90° as representative of the two characteristic types of noise signals found in the subsonic jet.

At this point it is prudent to briefly describe two statistical distribution functions that will be used several times in the subsequent analysis. The normal (or Gaussian) distribution is very common and describes quantities that fall symmetrically about some mean. The expression for the normal distribution is

$$N(x;\sigma,\mu) = \frac{1}{\sqrt{2\pi\sigma^2}} \exp\left[\frac{-(x-\mu)^2}{2\sigma^2}\right], \tag{6.1}$$

where μ is the mean (and also the mode) and σ^2 is the variance. If μ = 0 and σ = 1, the distribution is called the standard normal or unit normal.

The other distribution of note is the gamma distribution. The gamma distribution is a statistical distribution that arises from Poisson processes. In a Poisson process, the occurrences of events of interest are independent from one another and so these occurrences (e.g. wait times) are distributed randomly about some mean. The gamma distribution is described by the following function

$$G(x;\ell,\xi) = \frac{x^{\ell-1}\exp[-x/\xi]}{\Gamma[\ell]\xi^{\ell}}, \tag{6.2}$$

where ℓ and ξ are known as the shape and scale parameters, respectively, Γ is the gamma function, and x is the quantity of interest (e.g. the wait time before the occurrence of the next event). A few of the relevant properties of the gamma distribution are: 1) the mean occurs at $x = \ell\,\xi$, 2) the mode occurs at $x = (\ell - 1)\xi$, and 3) the variance of the distribution is $\ell\,\xi^2$.

In order to look at the scaling properties of these statistics as well as their relationship to the spectra, there are a few quantities that will need to be defined. The first is a non-dimensionalized time (τ). As seen in (6.3), time is non-dimensionalized using the jet diameter and either the jet exit velocity (resulting in a quantity that can be thought of as an inverse Strouhal number as already defined in §V) or the ambient speed of sound (in which case the quantity is an inverse Helmholtz number).

$$\tau_j = t\frac{U_j}{D} = \frac{1}{St_D} \qquad\qquad \tau_\infty = t\frac{a_\infty}{D} = \frac{1}{He} \tag{6.3}$$

VI.A. Amplitude Distributions

The first quantity to explore is the amplitude distribution of the peaks (A_i). In order to better understand the distribution of the peaks, it is prudent to first examine the distribution of amplitudes present in the original signal. The signal is quantized into 1000 amplitudes, normalized by the p_{RMS} of that particular signal, and the Probability Density Function (PDF) is computed (note that the area under the curve of a PDF should always be one). Several examples of the resulting distributions are shown in Fig. 4. In Fig. 4a, the PDF of the signal from the 30° microphone is shown for all cases—there are 21 curves of different colors in the figure. It is clear that, once normalized by p_{RMS}, the distribution of amplitudes collapses onto a single curve regardless of the jet size and operating conditions. The unit normal distribution curve is shown in Fig. 4a as a black line. In Fig. 4b, the PDF of the signal from all 24 microphones is shown for one jet with one operating condition along with the unit normal distribution curve. Again, total collapse is achieved. While it isn't possible to observe this from Fig. 4a as rendered, it is found that lower velocity jets have greater scatter about the unit normal curve while higher velocity jets, such as the one shown Fig. 4b, very closely hug the unit normal distribution. This change in scatter is true regardless of the jet diameter and temperature. It can therefore be concluded, as might be expected, that the distribution of amplitudes in any acoustic signal examined for this study obeys the unit normal distribution and the only controlling parameter is p_{RMS}.

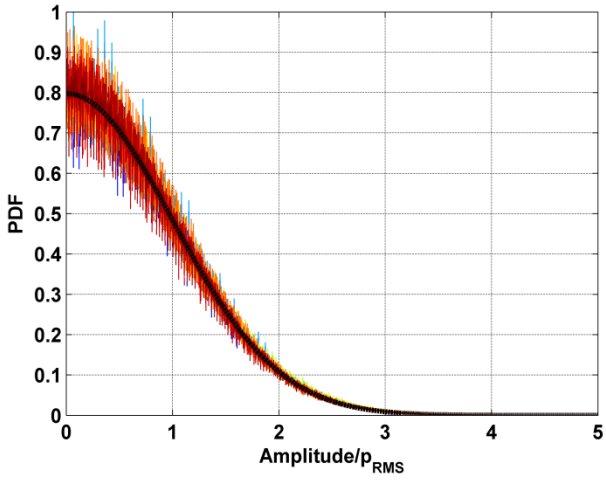

a) Total signal amplitude distribution for all cases at $\phi = 30°$

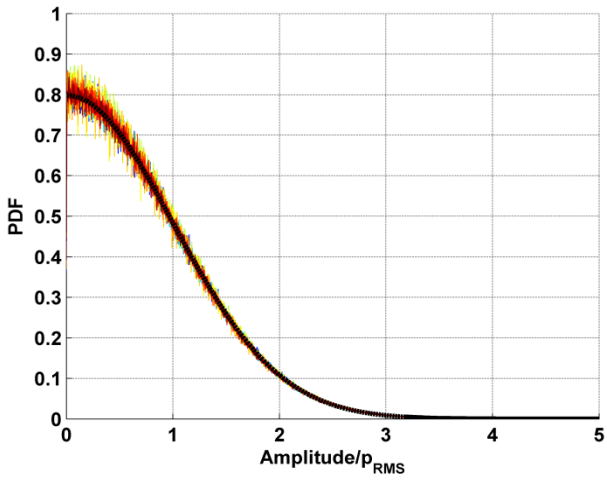

b) Total signal amplitude distribution for all polar angles operating conditions: $D = 2.54$ cm, TTR = 1.00, $M_a = 0.9$

Fig. 4: PDF of the amplitude of unaltered signals normalized by p_{RMS} for a given signal.

Looking at the peak amplitudes, the analysis becomes a bit more complicated. The PDF of the peak amplitudes for all 21 cases at 30° (all the cases used in Fig. 4a) is shown in Fig. 5. While good collapse is once again achieved, the distribution is not quite the unit normal. As should be expected, the distribution is sharply cut off at $1.5p_{RMS}$ as a consequence of the event definition. The best fit curve, however is a normal distribution with a standard deviation of $\sigma = 1.2$. If the PDF was determined from a signal that was simply truncated below $1.5p_{RMS}$, it would be equivalent to truncating the distribution in Fig. 4a at 1.5 and renormalizing for unit area. The departure from the unit normal can be explained by two factors. First, this distribution examines only the peak amplitudes. Points that would contribute to the distribution (i.e. all points in the signal above $1.5p_{RMS}$) are discarded unless they happen to be a peak. This is effectively like turning the gradual rise and fall of a peak into a delta function. The result of this process is that the distribution becomes slightly skewed toward values that are more likely to be peaks (i.e. larger values). Second, when two initially distinct peaks are determined to be overlapping, the two peaks are classified as a single event and only the larger peak is kept (see data extraction step 4 in §III). This also results in a preferential selection of larger amplitudes. The final result is that the distribution of peak amplitudes for all signals examined in this study (i.e. every polar angle for all cases) is described by the normal distribution with a σ of 1.2 and the value of p_{RMS} for a given signal.

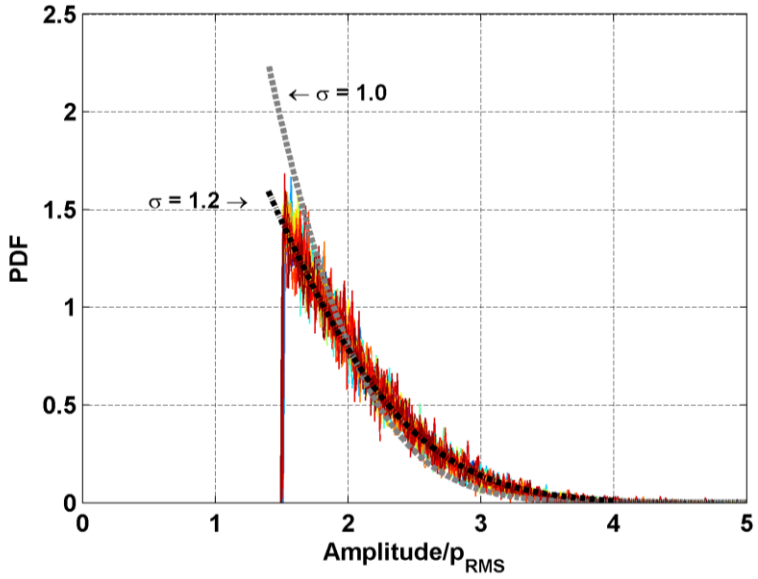

Fig. 5: PDF of peak amplitudes for all cases at $\phi = 30°$.

VI.B. Width Distributions

As discussed in §III, the event width (δt_i) is defined as the Full Width at Half Maximum (FWHM). The distribution of event widths provides information about the characteristic time-scale of the flow-field phenomenon that produced the acoustic event.

VI.B.1. 30°

The distributions of event widths for the various cases at the 30° microphone are shown in Fig. 6. In the unheated jet cases, the various velocities (acoustic Mach numbers) group very tightly according to jet diameter (Fig. 6a), indicating that the jet diameter is a representative length scale but the acoustic Mach number is not a representative velocity scale. However, upon close inspection (see Table 2) a trend with acoustic Mach number is detectable, but it is a weak dependence when compared to diameter and temperature variation. Given the very weak dependence on acoustic Mach number and thus jet velocity, it can also be concluded that the convective velocity would not be a proper scaling. In the case of heated jets, the acoustic Mach number dependence becomes significant. In the elevated temperature cases, however, there is a clear trend toward larger values with increasing temperature – especially for the lower velocity. This suggests that something in the noise producing dynamics changes at elevated temperatures and this new behavior is much more sensitive to the jet velocity. Applying the obvious first choice for scaling, inverse Strouhal number (τ_j), makes the distributions more disparate (see Fig. 6b), so it is not a good choice, as it was already determined that the jet velocity is not an appropriate velocity scale.

Kœnig *et al.* [37] observe these same trends by looking at spectral collapse. They note that Helmholtz scaling does the best job of collapsing the spectra at 30° for unheated jets of a single diameter while Strouhal number scaling does the best job for collapsing the hot jet cases. Their work to date does not include a parametric evaluation of jet diameter effects. It can be seen from Fig. 6 that Helmholtz scaling (lacking U_j dependence) would be a superior choice to Strouhal number scaling for the event widths in unheated jets, and that Strouhal number scaling is also inappropriate for the hot jets. In a related work Cavalieri *et al.* [42] propose that the superiority of Helmholtz scaling in the unheated jets is related to the non-compactness of the source associated with the azimuthally symmetric portion of the acoustic signal radiating to the low angles. They extend this idea to suggest that the source becomes more compact at elevated temperatures due to the disparity in the speed of sound between the jet core and the ambient. Cavalieri *et al.* [42] also notes that, while the axisymmetric mode scales with Helmholtz number, the first helical mode scales with Strouhal number and observe that the axisymmetric mode is only dominant at the low angles. While the explanations proposed by Kœnig *et al.* are interesting and warrant further investigation, they are still speculative at this time. An alternate possibility is that the hot jet introduces additional compressibility and/or viscosity considerations. The work of Kambe *et al.* on vortex collisions showed that the viscous dominated aspects of the collision process are significant to the noise produced in the collision [e.g. 43]. Given the significant changes in viscosity that occur as the jet is heated, it is possible that the collision dynamics are changing.

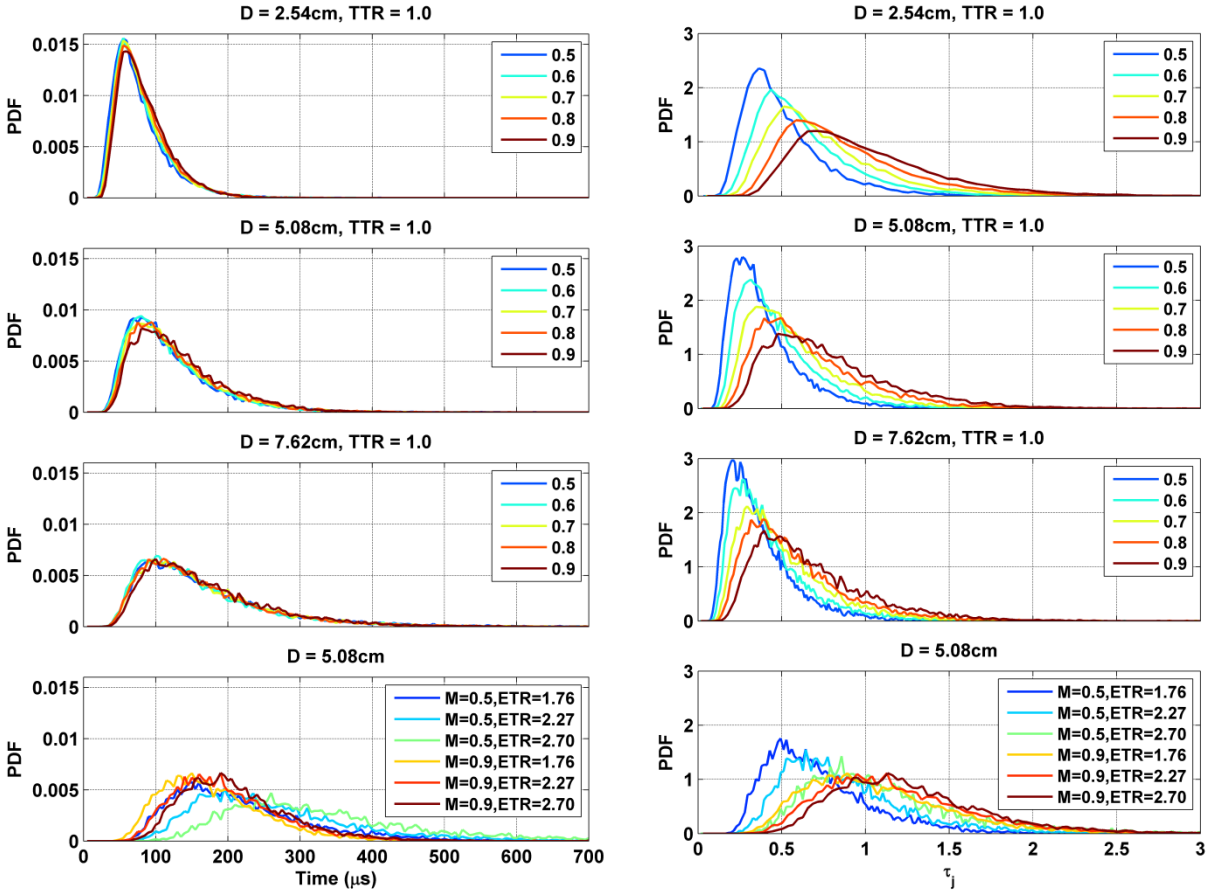

a) PDF with time abscissa **b)** PDF with scaled time, τ_j

Fig. 6: Distribution of event widths for all cases at $\phi = 30°$.

To a reader familiar with the gamma distribution, it should be apparent that these distributions are behaving at least somewhat like gamma distributions. Therefore, the distributions of event widths are fit with the gamma distribution and it is found that it is indeed a good fit (see Fig. 7) – the fit parameters are enumerated in Table 2. Additionally in Table 2, the mean event width ($\overline{\delta t}$) for the various cases is enumerated and the scaled values for both τ_j and τ_∞ are calculated. While not tabulated, the product of ℓ and ξ, the mean of the gamma distribution, is a pretty good match to the mean of the data (the maximum discrepancy is 10%). This agreement supports the statement that the gamma distribution is a good fit to the data. Detailed inspection of the distribution and best fit curves (not shown) confirms that these distributions are well described by the gamma distribution. It can be seen from the values in Table 2 that neither a Strouhal number nor a Helmholtz type scaling properly collapses the data. Looking at the general trend in the average width versus jet diameter or temperature for a given acoustic Mach number, the average event width appears to be scaling in a uniform manner, but conclusions should not be drawn until the polar angle dependence is examined (§VI.D).

Table 2: Various calculated quantities for the event width distributions at $\phi = 30°$.

	Jet Parameters			Gamma Parameters		Mean δt		
Case #	D (cm)	M_a	ETR	ℓ	ξ (μs)	Time (μs)	τ_j	τ_∞
1		0.5		5.75	12.36	77.7	0.51	1.02
2		0.6		6.16	11.94	80.0	0.63	1.05
3	2.54	0.7	~1	6.18	12.07	80.4	0.75	1.06
4		0.8		6.49	11.82	82.6	0.88	1.09
5		0.9		6.50	12.25	84.4	1.01	1.11
6		0.5		4.86	22.16	119.2	0.39	0.78
7		0.6		4.95	22.13	119.7	0.47	0.79
8	5.08	0.7	~1	4.99	22.91	124.1	0.57	0.82
9		0.8		4.99	23.54	127.4	0.67	0.84
10		0.9		5.00	24.82	132.3	0.78	0.87
11		0.5		4.18	35.97	167.9	0.37	0.74
12		0.6		4.33	33.31	161.0	0.42	0.71
13	7.62	0.7	~1	4.27	35.42	165.4	0.51	0.72
14		0.8		4.37	34.30	163.3	0.57	0.72
15		0.9		4.54	34.68	170.3	0.67	0.75
16		0.5	1.76	5.89	34.72	218.6	0.72	1.44
17		0.9	1.76	6.34	27.71	180.5	1.07	1.19
18	5.08	0.5	2.27	6.61	37.58	263.7	0.87	1.73
19		0.9	2.27	7.66	25.20	198.8	1.18	1.31
20		0.5	2.70	7.19	43.52	337.5	1.11	2.22
21		0.9	2.70	8.83	23.28	211.8	1.26	1.39

To examine the relationship between the distributions and the trends in the mean width, the distribution widths were scaled by their respective means and the PDFs for all cases are shown in Fig. 7. Additionally, a gamma distribution curve based on the averaged gamma parameters ($\ell = 5.72$ & $\xi = 0.17$) is shown as a black dashed line. It should be noted that ξ must be non-dimensionalized by the mean event width for a given case before averaging. While the collapse is not quite as good as the amplitude distributions, it is still sufficient to say that the mean event width is the controlling parameter in the distribution of event widths. Once the mean value is known, the entire distribution can be reasonably well predicted based on universal values for $\ell \approx 5.72$ and $\xi \approx 0.17$.

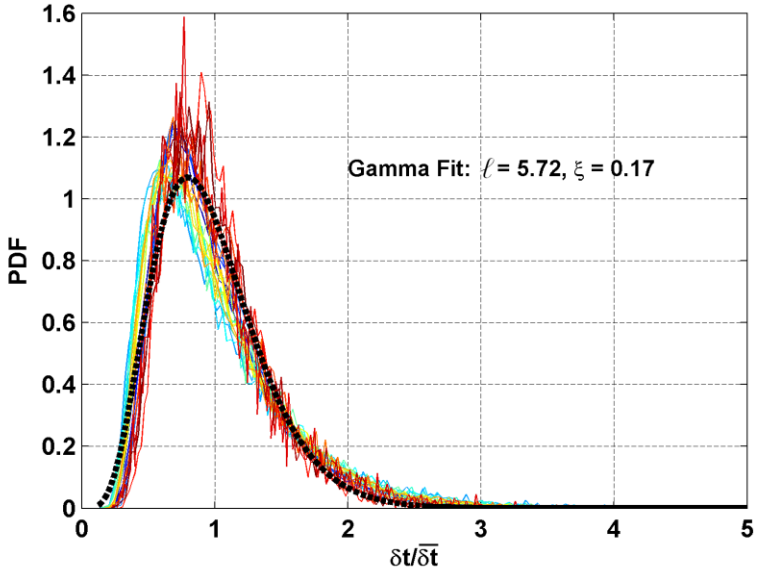

Fig. 7: Distribution of event widths normalized by their respective means for data at $\phi = 30°$.

There are several conclusions to draw from these results.

1. The mechanism that produces these noise events is not particularly sensitive to jet velocity, but it is sensitive to diameter and temperature. Furthermore, the changes in the distributions with jet diameter are not directly proportional to the jet diameter.
2. The agreement of the data with a gamma distribution indicates that the lifetimes or time-scales of these events are uncorrelated (i.e. independent from one another). This implies that the source mechanism of these events is sufficiently independent from one event to the next making it unique. This makes sense since the source flow-field is a highly turbulent flow.
3. There exists only one controlling parameter in the distribution (in this case the mean width). Once that parameter is known, the entire distribution is known – along with the universal values of ℓ and ξ.

If these results are interpreted within the context of vortex sound as discussed in §II.A, some interesting correlations are found. In Kambe's work on vortex ring collisions, it was found that the characteristic lifetime of the noise generated by the collision grew as R_o/U, where R_o is the initial radius of the vortex ring. The present results show that the characteristic lifetime (i.e. width) of the noise events in the jet are similarly scaling with jet size (or the nozzle exit diameter). Since Kambe's work uses the collision velocity U, it is difficult to discuss the relationship between his experiments and present trends except to speculate that it might indicate that the collision (loosely interpreted as the interaction of structures) speed doesn't change significantly with increasing jet velocity in the unheated jets.

VI.B.2. 90°

The distributions of event widths for the various cases at the 90° microphone are shown in Fig. 8. The marked grid-points on the abscissa are spaced at the resolution of the analysis (5 μs) – there is one data point per grid marker for these distributions. Per the definition of the event width, the minimum allowed event width is 10 μs. Regardless of operating conditions, the peak of the distribution occurs at a very short time and it is also fairly constant. The peaks in all of the cases are separated by no more than four data points with the largest peak width being only 40 μs (eight data points). The mean event widths are enumerated in Table 3. The mean event widths have a slightly larger range (7 data points), but the result is quite clear. The events at the sideline and upstream angles based on the definition chosen in this paper are rapid oscillations whose characteristics are dictated, not by the flow, but primarily by the sampling rate of the data.

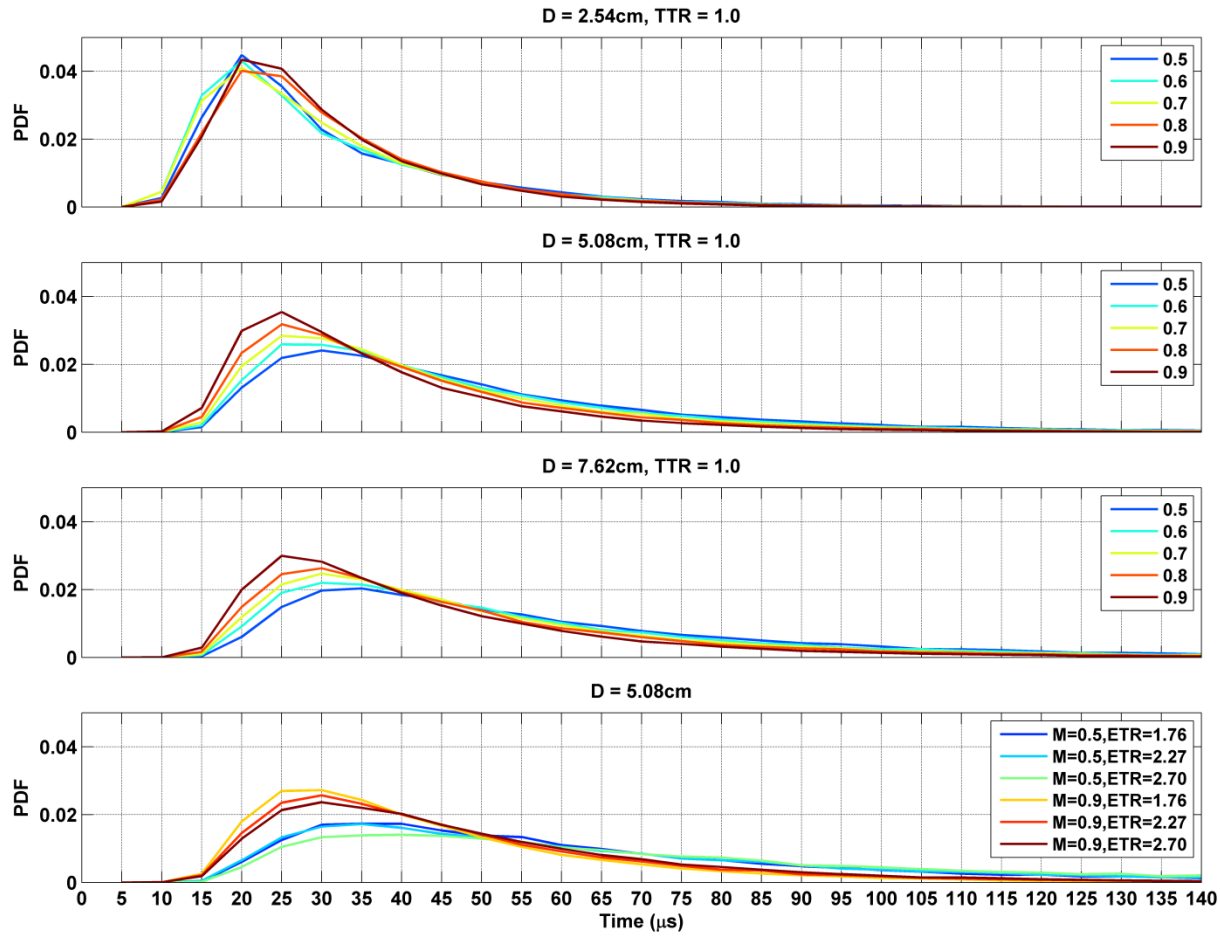

Fig. 8: Distribution of event widths for all cases at $\phi = 90°$.

Table 3: Mean event width for all cases at $\phi = 90°$.

Case Number	1	2	3	4	5	6	7	8	9	10
Mean Width (μs)	32	30	30	31	30	49	46	43	41	38

Case Number	11	12	13	14	15	16	17	18	19	20	21
Mean Width (μs)	59	54	50	47	43	63	44	65	47	75	49

The result here confirms and quantifies the conclusion reached in §V and also agrees with the assessment of spectral analysis that the sound radiated in sideline and upstream directions has at least some of the characteristics of white noise. These events are fundamentally different from those at low angles and are very nearly delta functions with respect to the sampling rate. Furthermore, the sampling properties of the signals make a competent analysis of these events impossible – to determine if there is any significant structure in these signals would likely require increasing the sampling rates by at least a factor of 5. One last observation is that the event width distributions at 90° can also be described adequately by a gamma distribution, but this is not of any real use given the preceding discussion. Since it has been established that the event definition and analysis process cannot provide an informative description of sideline and upstream noise, further analysis of these radiation directions will be more restricted.

VI.B.3. Joint PDF—Amplitude and Width – 30°

One might expect there to be a relationship between the amplitude and width of an event. To explore this possibility the joint PDF of the two variables is calculated for the 30° data. Based on §VI.B.2 it is concluded that it is not useful to analyze the sideline and upstream angles. The distributions are normalized so that there is unit

volume under the surface. Based on the scaling characteristics determined in §VI.A and §VI.B, the distributions are presented with the event widths (δt) normalized by the mean event width and binned at the resolution of the data (5 μs). The peak amplitude (p_{peak}) is normalized by the RMS pressure and the data are divided into 70 bins between $1.4p_{RMS}$ and $3.5p_{RMS}$.

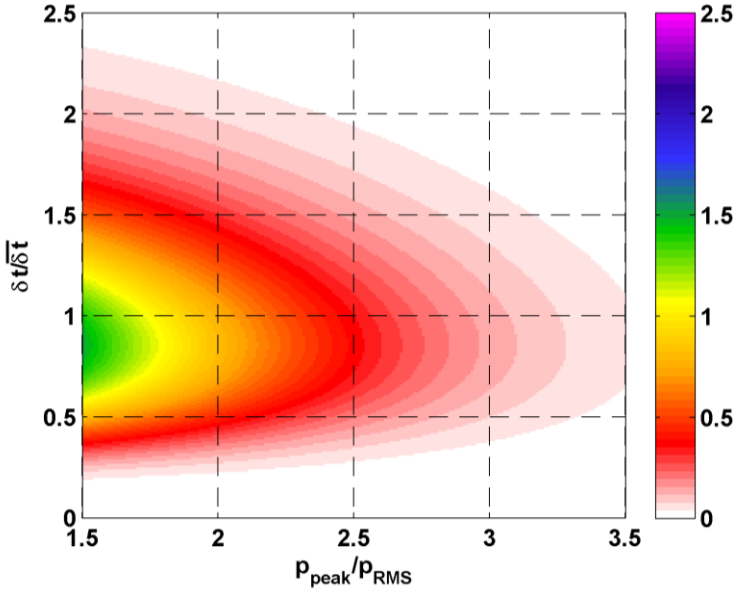

Fig. 9: Joint PDF for event width ($\ell = 6$, $\xi = 0.17$) and amplitude ($\sigma = 1.2$) assuming the two quantities are independent random variables.

If the two variables are statistically independent, the combination of a given amplitude and width would simply be the product of the distributions for the two variables. Since universal distributions for these variables have already been established, it is easy to calculate what the independent joint PDF would look like. The independent joint PDF is shown in Fig. 9 using $\ell = 6$, $\xi = 0.17$, and $\sigma = 1.2$. As expected, the most probable event width lies on a horizontal line at a value of 0.85. Another possibility is that the width and amplitude are related by some geometric relationship. A simple example of such a relationship is that of the width and height of an isosceles triangle with a constant spreading angle. In this simple example, fractional changes in width are equal to fractional changes in height (i.e. if the height doubles, the width doubles).

The joint PDFs for several cases are shown in Fig. 10. Subfigures a-c show the variation with diameter, d-f show the variation with acoustic Mach number, g-i show the variation with ETR at $M_a = 0.5$, and j-l shown the variation with ETR at $M_a = 0.9$. There is very little change in the distribution with diameter – the peak of the distribution decreases slightly with increasing diameter. There is essentially no change in the distribution width acoustic Mach number; consistent with the conclusions from §VI.B. Heating does produce noticeable changes. In both acoustic Mach numbers, increasing the temperature causes the distribution to elongate in the p_{peak} direction (i.e. for a given width, larger amplitude events become more probable with increasing temperature) while the width dimension is relatively fixed. The elongation isn't extreme, but it is significant.

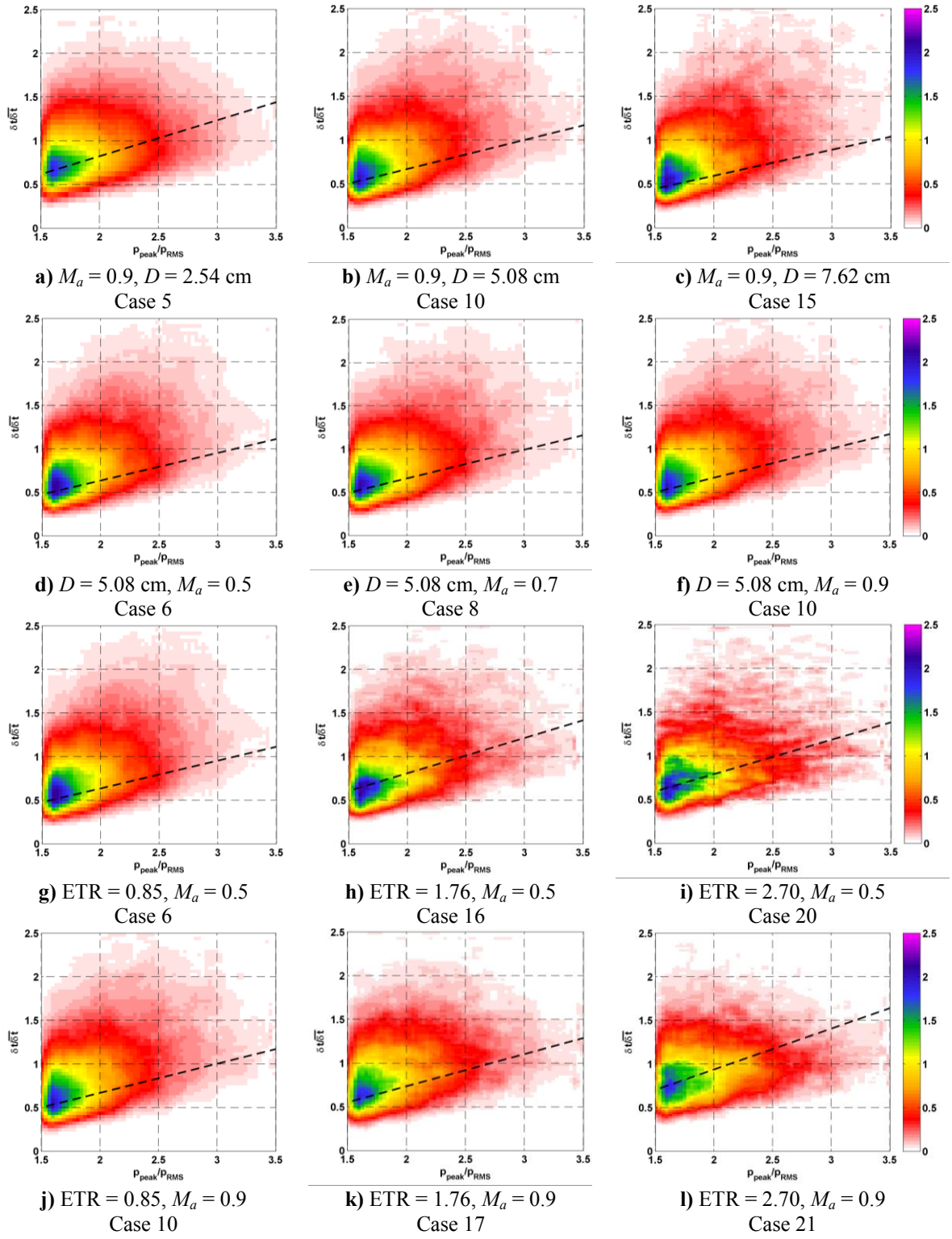

a) $M_a = 0.9$, $D = 2.54$ cm Case 5 **b)** $M_a = 0.9$, $D = 5.08$ cm Case 10 **c)** $M_a = 0.9$, $D = 7.62$ cm Case 15

d) $D = 5.08$ cm, $M_a = 0.5$ Case 6 **e)** $D = 5.08$ cm, $M_a = 0.7$ Case 8 **f)** $D = 5.08$ cm, $M_a = 0.9$ Case 10

g) ETR = 0.85, $M_a = 0.5$ Case 6 **h)** ETR = 1.76, $M_a = 0.5$ Case 16 **i)** ETR = 2.70, $M_a = 0.5$ Case 20

j) ETR = 0.85, $M_a = 0.9$ Case 10 **k)** ETR = 1.76, $M_a = 0.9$ Case 17 **l)** ETR = 2.70, $M_a = 0.9$ Case 21

Fig. 10: Joint probability density functions of event amplitude and width for several operating conditions at ϕ = 30°.

It is immediately clear that the width and the amplitude are not independent, but determining the nature of the dependence is considerably more difficult. The dashed line is the doubling line (i.e. the width doubles when the amplitude doubles) that passes through the peak of the distribution. For any given amplitude, the peak width follows the doubling line quite well across all of the cases. If the width and amplitude were deterministically linked and all

events had the same spreading angle, then the distribution should tightly follow the dashed line on the figures. Since, however, there is no reasonable expectation (as seen from the broad variation in widths for any given amplitude) for all events (even of a single amplitude) to have the same spreading angle, it is concluded that the two quantities are correlated, but not deterministically. The amplitude seems to dictate a minimum width, but allows a range of widths above this. Also, the consistent match between the doubling line and the peak of the distribution suggests that there is a characteristic shape to the events that scales depending on the amount of energy in the event. One other conclusion is that the elongation of the distribution in the p_{peak} direction with heating indicates that the amplitude and width are becoming less correlated.

VI.C. Intermittence Distributions – 30°

The last characteristic of the noise event needed to complete the picture is the time between isolated events (the intermittence). It should be noted that this intermittence is not related to the fluid dynamics concept of turbulence "intermittency" [44, pp.167-173]. Based on the preceding discussion, only 30° is analyzed as the representative sample of low angle noise. Generally, the N^{th} order intermittence can be written as

$$\Delta T_i^{(N)} = T_i - T_{i-N}, \tag{6.4}$$

where T_i is the temporal location of the i^{th} event peak as discussed in §III. The distribution of the N^{th} order intermittence is then found by calculating the histogram of the set $\left\{\Delta T_i^{(N)}\right\}_i$. As can be seen in the sample signals plotted in Fig. 2, the true nature of these noise events often includes at least one positive and one negative swing beyond the $1.5p_{RMS}$ threshold. Since these are identified as distinct events, an indiscriminate calculation of the intermittence distribution would likely be skewed by the statistics regarding the spacing of these peak-to-peak swings. This peak-to-peak interval information is characterized by the event widths, so it is redundant to include it here. The simplest solution to this issue is to look at peaks of one sign only and this is the method that will be used. The results from looking at only positive peaks and then only negative peaks can be averaged together to conserve the statistical population size of the analysis. Since at least some events consist of multiple positive and negative swings, it is also prudent to average over several orders of intermittence. Based on the assumption that the $N = 2$ distribution should have a characteristic value approximately twice that of the $N = 1$ distribution, the average of M orders of the N^{th} order distribution ($H_j^{(N)}$) can be calculated as

$$\Upsilon_j = \frac{1}{M}\sum_{N=1}^{M} NH_{jN}^{(N)}, \tag{6.5}$$

where j denotes the j^{th} bin of the distribution. The N^{th} order distribution is down-sampled by a factor of N (indicated by the subscript jN) and scaled by a factor of N to conserve the area under the curve. The down-sampled and scaled distributions can then be point-by-point averaged.

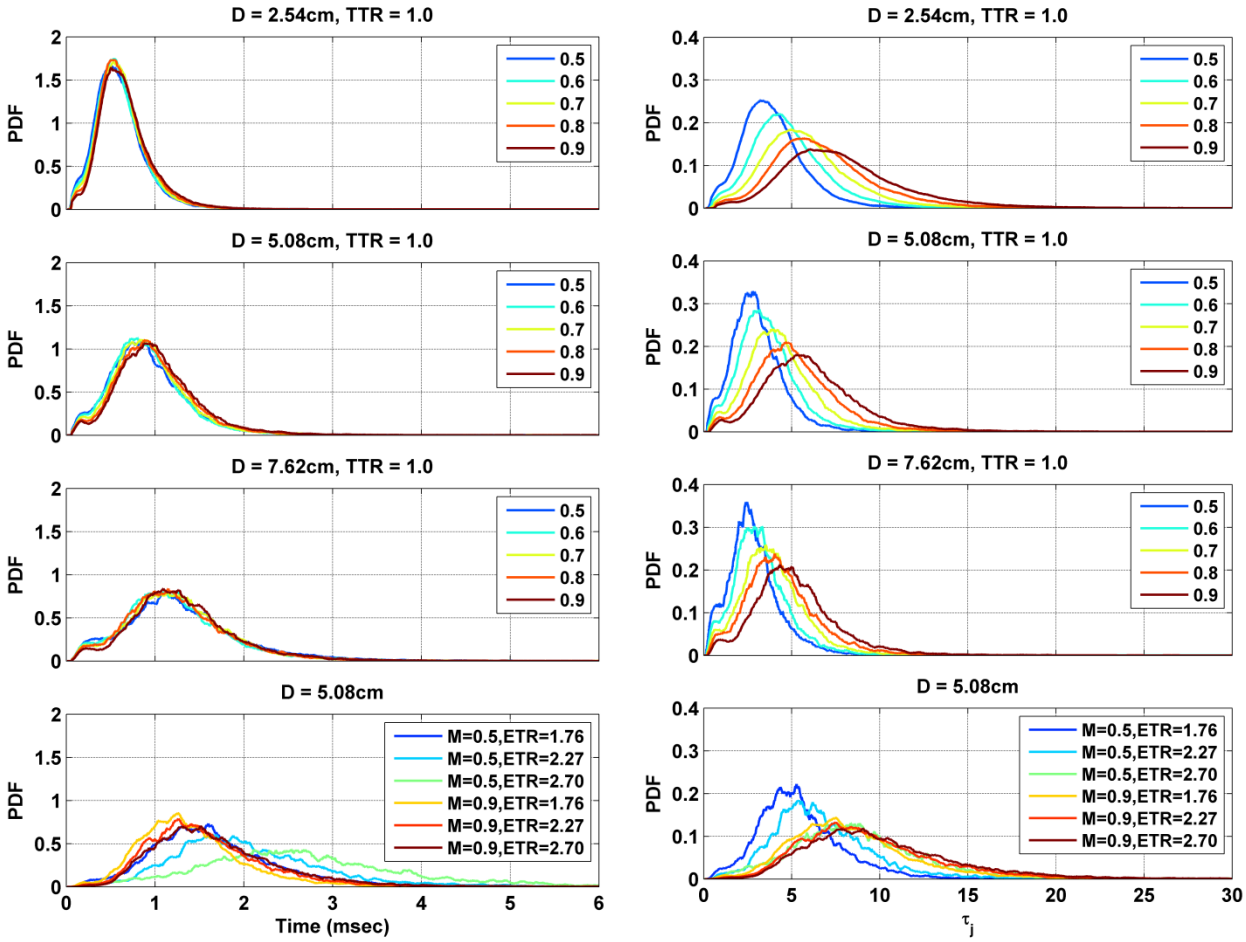

a) Unscaled distributions **b)** Scaled time as τ_j

Fig. 11: Distribution of events intermittence for all cases at ϕ = 30°.

The distributions of event intermittence are shown for the 30° data in Fig. 11. It is clear that, apart from the time scale, the distributions of event intermittence behave very similarly to the event width. The small secondary peak close to the origin is evidence of the peak-to-peak swing time scale already discussed. A relatively weak dependence on jet velocity for the unheated jets is observed, as are strong dependencies on jet diameter and temperature. In the hot jet cases, a velocity dependence is also present. This same behavior was observed in the wavelet transform analysis of Kœnig *et al.* [37]. They indirectly infer a change in the intermittence through changes in the fraction of energy retained when filtering at the same threshold in the wavelet domain. Once again, the data lends itself to description by the gamma distribution. The best fit gamma parameters as well as the mean event intermittence ($\overline{\Delta T}$) are listed in Table 4. The mean of the best fit gamma distribution matches the empirical mean pretty well (maximum discrepancy is 4%) and a detailed examination of the best fit curves (not shown) shows that the data is indeed well described by the gamma distribution. The degree of similarity in the trends between event width and intermittence is actually quite high. If the ratio of the mean event width to the mean intermittence is calculated for all cases, the average and standard deviation of that set of ratios is $\overline{\delta t}/\overline{\Delta T}$ = 0.128 ± 0.002. This suggests that the periodicity of events and the lifetime of those events are strongly related. Additionally, the order of magnitude disparity in these quantities is in contravention to the sinusoidal behavior of typical wave-packet models.

Table 4: Various calculated quantities for the event intermittence distributions at $\phi = 30°$.

	Jet Parameters			Gamma Parameters		Mean ΔT		
Case #	D (cm)	M_a	ETR	ℓ	ξ (μs)	Time (msec)	St_D	He
1		0.5		5.53	109.50	0.60	0.25	0.13
2		0.6		5.99	102.71	0.61	0.20	0.12
3	2.54	0.7	~1	6.29	99.87	0.63	0.17	0.12
4		0.8		6.60	95.92	0.65	0.15	0.12
5		0.9		6.32	103.45	0.67	0.13	0.11
6		0.5		5.08	185.42	0.92	0.33	0.17
7		0.6		5.69	163.21	0.92	0.27	0.16
8	5.08	0.7	~1	6.04	159.12	0.95	0.23	0.16
9		0.8		6.03	166.03	0.98	0.19	0.15
10		0.9		6.34	163.43	1.05	0.16	0.15
11		0.5		4.59	294.80	1.30	0.35	0.18
12		0.6		5.18	244.33	1.24	0.31	0.18
13	7.62	0.7	~1	5.51	238.54	1.28	0.25	0.18
14		0.8		5.41	236.62	1.27	0.22	0.18
15		0.9		6.26	212.27	1.31	0.19	0.17
16		0.5	1.76	6.54	252.91	1.71	0.18	0.09
17		0.9	1.76	6.63	210.56	1.43	0.12	0.11
18	5.08	0.5	2.27	6.84	294.60	2.08	0.15	0.07
19		0.9	2.27	6.56	234.35	1.60	0.11	0.10
20		0.5	2.70	6.24	437.32	2.73	0.11	0.06
21		0.9	2.70	6.37	258.76	1.70	0.10	0.09

Following the same approach as in §VI.B.1, the intermittence distributions are scaled by their respective means and plotted in Fig. 12 along with a gamma distribution curve given by the average gamma parameters ($\ell = 6.0$ & $\xi = 0.17$). With the mean quantity scaled out, the distribution of the event intermittence is also seen to be universal and to be well predicted by a gamma distribution. These noise events are independent; that is, the occurrence of one event does not influence the occurrence of another. This conclusion was also reached by Guj *et al.* [32]. Again, these results are in stark contrast to typical wave-packet models that are based on a nearly sinusoidal ansatz. Lastly, there is only one controlling parameter on the distribution (the mean) and, once known, the entire distribution may be predicted. It is also worth noting that, in addition to the link between their mean values as already discussed, the distribution of event intermittence has very similar gamma parameters to the event width distribution.

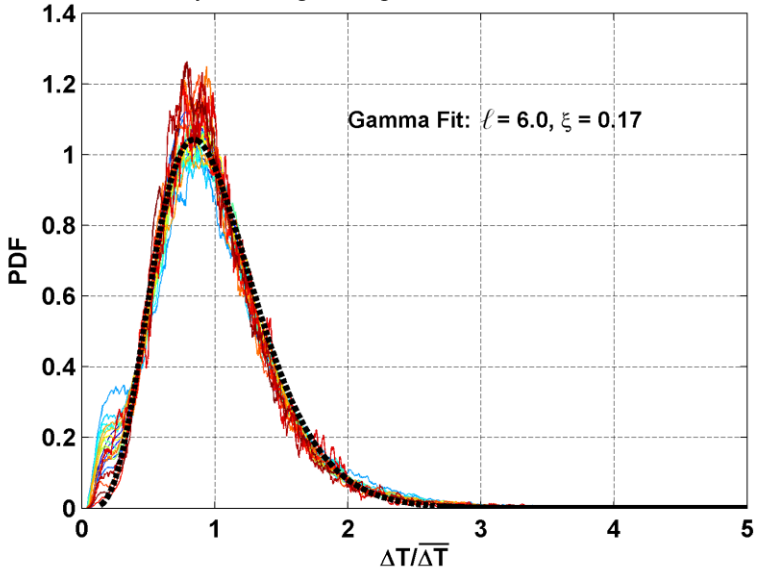

Fig. 12: Intermittence distributions normalized by their respective means for data at $\phi = 30°$.

The reader may have already noticed that the mean intermittence has something important to say in relation to the spectra. As mentioned in §II.B, Kœnig *et al.* [37] noted that scaling the frequency axis into Helmholtz number can achieve better spectral collapse for varying acoustic Mach number than Strouhal number scaling in an unheated jet. This implies that the spectral characteristics depend, at most, weakly on the jet velocity. Inspection of the 30° spectra on a Helmholtz number axis in Fig. 13 reveals a fairly constant value of the peak Helmholtz numbers irrespective of acoustic Mach number for the unheated jets. This is similar to the trends observed in the event intermittence as well as event widths. The amplitudes of the spectral peaks in Fig. 13 are artificially aligned. The collapse is quite similar to that observed in Kœnig *et al.* [37]. The value of the mean intermittence, converted into Helmholtz number, is marked with triangles. The mean intermittence does a pretty good job of predicting the peak in the spectrum. The prediction is not quite as good for the low-speed 7.62 cm cases. This may be due to the properties of the anechoic chamber combined with the frequencies of the jet. As discussed in §IV, the anechoic chamber is effective down to about 200 Hz. The peak frequencies of the 7.62 cm jet are close to the limits of the chamber so it is possible that the results are being skewed by reflections. In the elevated temperature cases, prediction is pretty good for the low-speed cases, but is a bit low for the high-speed cases. It is possible that combustor noise is skewing these results. Given the additional complexities of the hot jet cases, the agreement is decent. The consistency of the mean intermittence with the spectral peak indicates that the quasi-periodicity of these events is what creates the spectral peak.

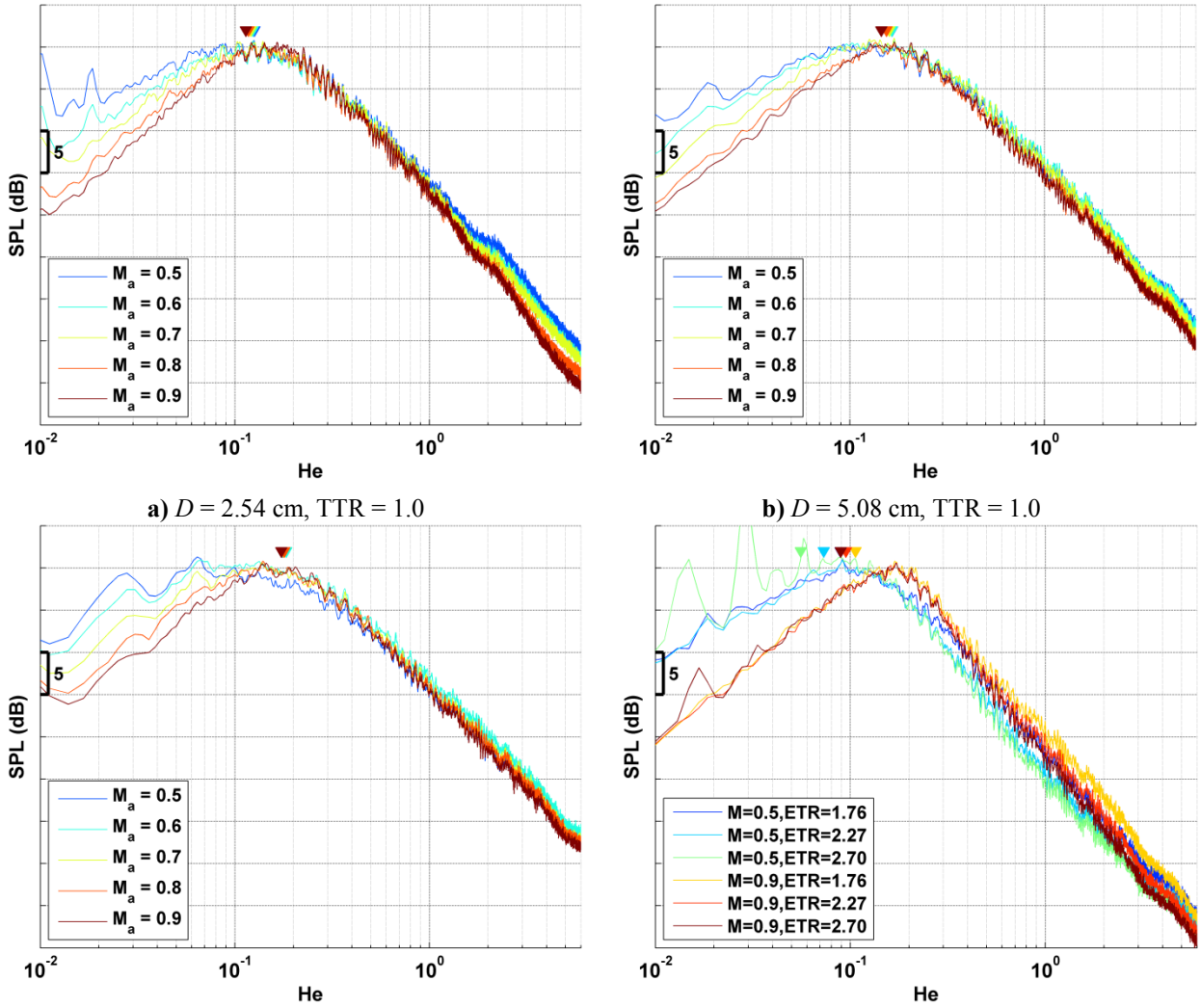

a) D = 2.54 cm, TTR = 1.0

b) D = 5.08 cm, TTR = 1.0

c) D = 7.62, TTR = 1.0

d) D = 5.08 cm, elevated temperatures

Fig. 13: Spectra at ϕ = 30° showing the predictive capability of the mean intermittence.

VI.D. Directivity of Mean Event Width

Analysis of the 30° and 90° microphone signals has shown that there are a few important variables in these noise events. With that information, more polar angles are examined. The mean width ($\overline{\delta t}$) directivity for the five acoustic Mach numbers in the unheated jet is shown in Fig. 14a. The first thing to note is that there is very little variation in this directivity for the different acoustic Mach numbers. Apart from some subtle trends with velocity that have already been discussed in more detail in §VI.B, these directivity patterns are essentially identical. There is some apparent variation in the upstream angles, but as already discussed, the information from these directions is of limited use due to the nature of the signals. There is also more variation in the 15° microphone, but that might be expected given the close proximity to the jet plume. Another important observation is that beyond 55° the mean width becomes constant. This indicates (as can be confirmed by examination of the spectra) that the noise radiated to angles of 60° and higher has a similar nature. It is also found that the gamma parameters that describe the distributions follow similar trends with polar angle. The shape parameter (ℓ) changes much less than the rate parameter (ξ). The shape of the gamma distribution changes gradually with polar angle as the noise signal transitions from an intermittent nature to a more white noise type nature.

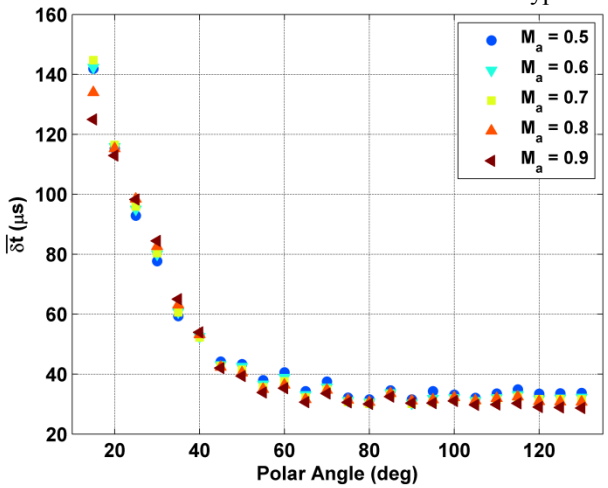

a) Various Mach numbers for D = 2.54 cm & TTR = 1.0

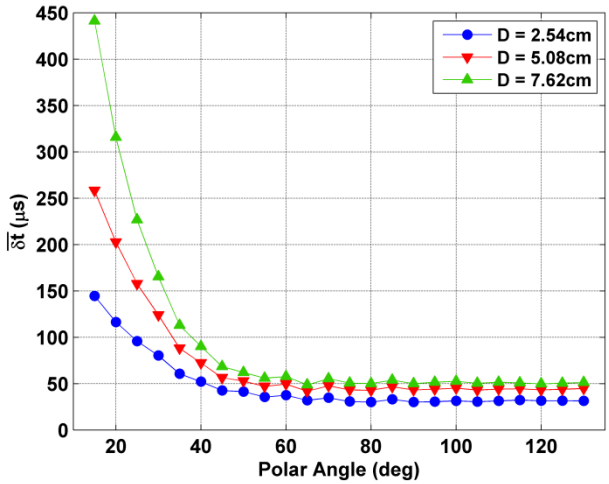

b) Various diameters for M_a = 0.7 & TTR = 1.0

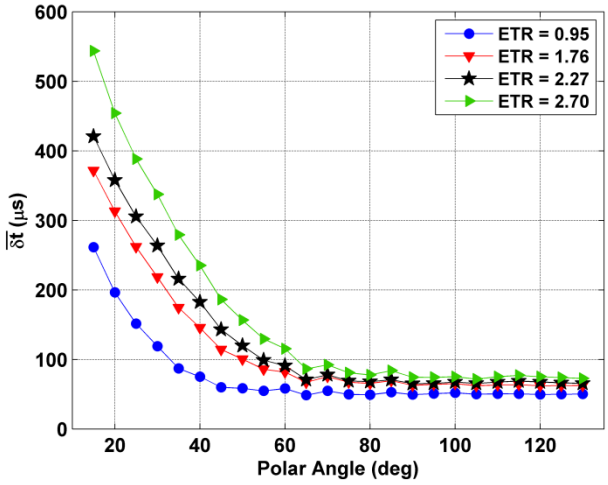

c) Various exit temperature ratios for D = 5.08 cm & M_a = 0.5

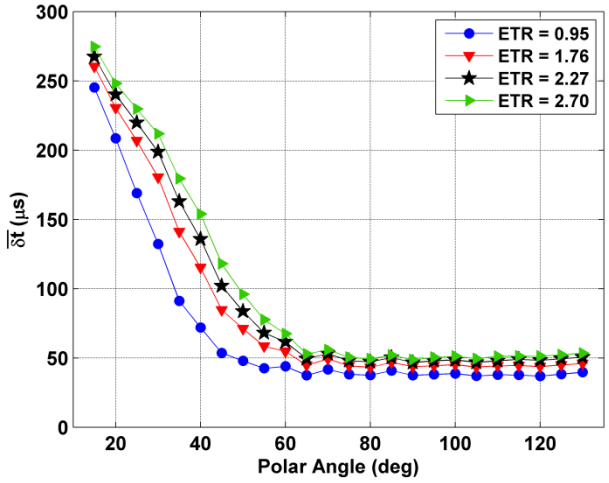

d) Various exit temperature ratios for D = 5.08 cm & M_a = 0.9

Fig. 14: Directivity patterns for mean event width.

The directivity of the mean width for the three jet diameters is shown for the unheated jet and the middle acoustic Mach number (M_a = 0.7) in Fig. 14b. While the sideline and upstream angles change very little, it is clear that the mean width has a coupled dependence on the jet diameter and polar angle for the low angle noise. The dependence on the jet temperature is also complex (Fig. 14 c & d). Again there is very little change in the sideline

and upstream angles. The mean width in the transition angles (ϕ = 40° to 60°) changes more rapidly as the jet gets hotter. The low angles (ϕ = 15° to 35°), however, have a fairly constant slope with their absolute values being dictated by the changes in the transition angles. Lastly, it is seen that a larger jet velocity significantly suppresses these trends with temperature. It is not clear at this time how to construct an appropriate scaling scheme to account for these trends. It is likely that a much more extensive data set would be required to understand it fully.

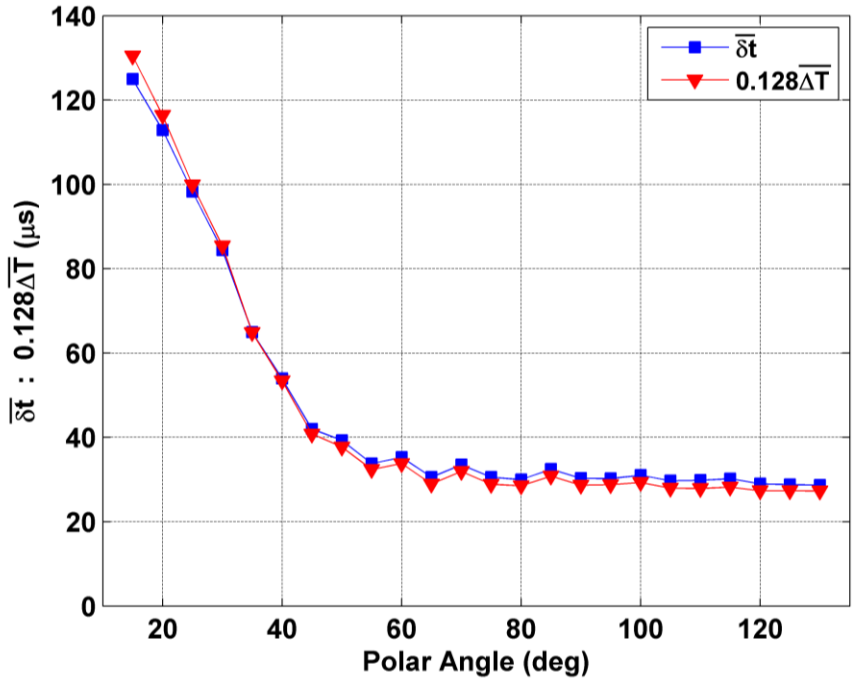

Fig. 15: Directivity pattern of mean width and intermittence for Case 5 (D = 2.54 cm, M_a = 0.9, & TTR = 1.0).

The mean width ($\overline{\delta t}$) and intermittence ($\overline{\Delta T}$) are shown vs. polar angle for case number 5 (D = 2.54 cm, M_a = 0.9, TTR = 1.0) in Fig. 15 where the mean intermittence has been scaled by 0.128 based on the conclusion reached in §VI.C. Case 5 was chosen as a representative sample. This shows that there is a strong and consistent relationship between the mean event width and intermittence regardless of polar angle – further supporting the idea that the two are dynamically linked in some way. One possible explanation for this link can be found by looking at vortex sound. Vortex sound, as discussed in §II.A, has shown that width of a noise event created by colliding vortices scales with the size of the vortices. The size of the typical vortex in the jet is dictated partly by the frequency with which they occur. Thus the frequency of occurrence (the intermittence) could be linked to the width of the noise event through the size of the typical vortex if it is found that vortex collision/decay processes are indeed responsible for these noise events.

Returning to the comparison of the mean intermittence to the spectral peak (Fig. 13), it is found that, in terms of Helmholtz number, the spectral peak frequency at the low angles is fairly constant for a given jet diameter and polar angle in the unheated jet. In contrast, the spectral peak Strouhal number for angles above about 50° is pretty constant. While there aren't any additional figures (in the interest of brevity) showing direct comparisons for polar angles other than 30° (see Fig. 13), the mean intermittence is a pretty good match to the spectral peak for the low angles. On the range ϕ = 15° to 40°, the prediction is generally quite good. For higher polar angles, the peak frequency is consistently over-predicted, but as already discussed, this analysis does not expect to correctly predict the properties of radiation to the sideline and upstream angles.

VI.E. Averaged Event Waveform

Up to this point, the data have revealed several important things about the nature of jet noise. One feature that has been notably absent is the shape of the typical noise event. While the instantaneous waveform changes, the shape obtained by averaging many events can provide some useful information. Averaging is performed on the raw data by extracting a portion of raw data around each identified event that is ten times the calculated width of that event. Note that this averaging does not utilize any wavelet fitting as discussed in §V. Events with negative peak

amplitude are inverted. All events are aligned in time for a coincident peak and then averaged. A representative sample of this result is shown in Fig. 16a for Case 5 (D = 2.54 cm, M_a = 0.9, TTR = 1.0). While only one example is shown, the subsequent discussion and analysis has been confirmed to be valid across all cases. This figure shows several features already identified in the previous sections (e.g. the typical event width at low angles is larger than sideline angles, angles greater than about ϕ = 50°-60° have consistent characteristics, etc.). The main piece of additional information provided by the averaged waveform is that the low angles contain at least one statistically significant negative swing associated with the positive swing. Conversely, the sideline averaged waveforms have no statistically significant negative swing.

It is important to note that this averaged waveform is not a good representation of the instantaneous signal. If the instantaneous waveform consisted of three alternating lobes, as the averaged waveform suggests, the intermittence analysis should have strongly detected a characteristic time ΔT on the order of δt. One possible waveform is an event containing one positive and one negative swing, but not necessarily in that order (referred to as a one-and-one waveform) – shown as item A in the cartoon in Fig. 17. This waveform can explain many of the observed behaviors.

1. The one-and-one waveform is consistent with the averaged waveform. There is no way to separate the cases where the negative swing precedes the positive or vice versa without assuming something about the governing dynamics that produced the noise event (see cartoon items A and B). If, during averaging, the positive peaks of A and B are aligned and averaged, the result would be a symmetric waveform like that shown in the cartoon which matches the shape of the average waveform in Fig. 16.
2. The existence of negative lobes in the average waveform indicates that there must be some swing of opposite sign associated with the primary peak. If the typical instantaneous event had no negative swing (e.g. Gaussian), the average waveform would not have negative lobes.
3. In the cartoon, the amplitudes of the negative lobes on the average waveform are half the amplitude of the positive lobe. In Fig. 16a, however, the secondary swing is of considerably reduced amplitude. This is an artifact of the averaging. There are events of all different widths averaged together with one enforced point of coincidence (time equals zero). The averaged waveform, therefore, becomes increasingly smeared with increasing distance from the enforced point of coincidence. For any given event, it is therefore possible that the negative swing would have amplitude comparable to the positive swing. In an effort to explore the impact of this averaging, the events used to create the average waveform for 30° in Fig. 16a were scaled to remove the effect of varying amplitude and width before averaging. The time axis of each event was normalized by the event width (δt) and the peak amplitude of the event was scaled to one. The normalized events were averaged and the result is shown in Fig. 16b along with the waveform that would result from applying the same averaging procedure to the proposed one-and-one instantaneous waveform. It is clear that, while there is a basic consistency, many of the details are different. This suggests that either the shape of the typical event is more complex than the simple model used in this section or that there multiple types of events present in the signal. The present model, however, is still acceptable for the analysis discussed here – a more complex waveform isn't needed to discuss the basic nature of the event dynamics and, if there are multiple event types present, the presence of the negative lobes indicates that the event type under discussion must be prevalent.
4. From Table 2 the average event width at 30° is $\overline{\delta t}$ = 84 μs (which agrees well with the averaged waveform). The minimum in the averaged waveform occurs at 170 μs. If it is assumed that the instantaneous waveform is a one-and-one event, a crude model of this waveform is two adjacent isosceles triangles of equal dimensions with one pointed up and the other pointed down. In this case, the geometry says that the distance between the two peaks is $2\,\overline{\delta t}$ which is a very good match to the location of the averaged waveform minimum.

Based on these findings, it is reasonable to conclude that the one-and-one waveform may be a reasonable representation of the instantaneous noise event. This could also explain portions of signal with more than one positive and negative swing as being sequential occurrences of this basic signature.

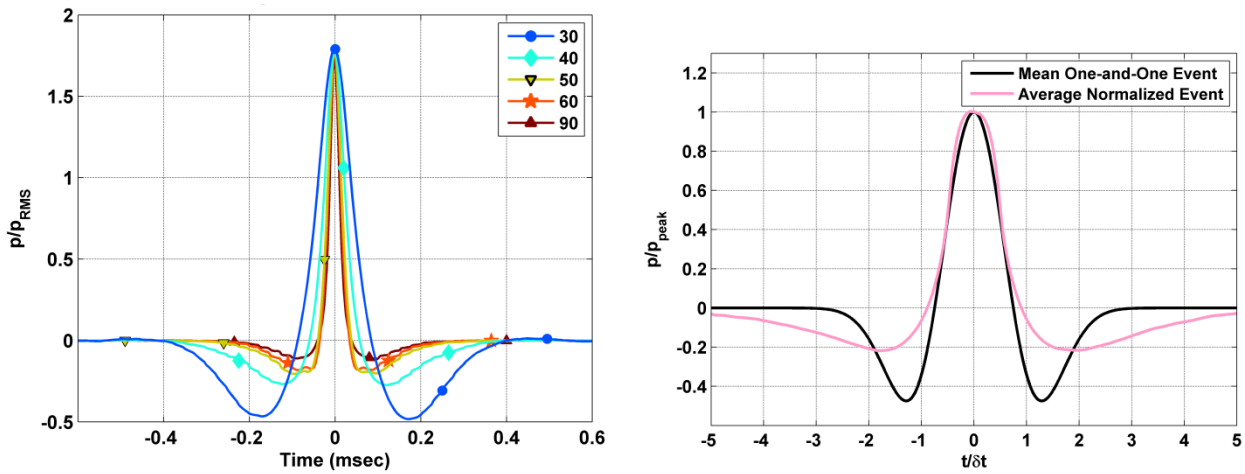

a) Un-normalized

b) $\phi = 30°$ events normalized by width and amplitude before averaging.

Fig. 16: Averaged event waveform for several polar angles in Case 5 (D = 2.54 cm, M_a = 0.9, TTR = 1.0).

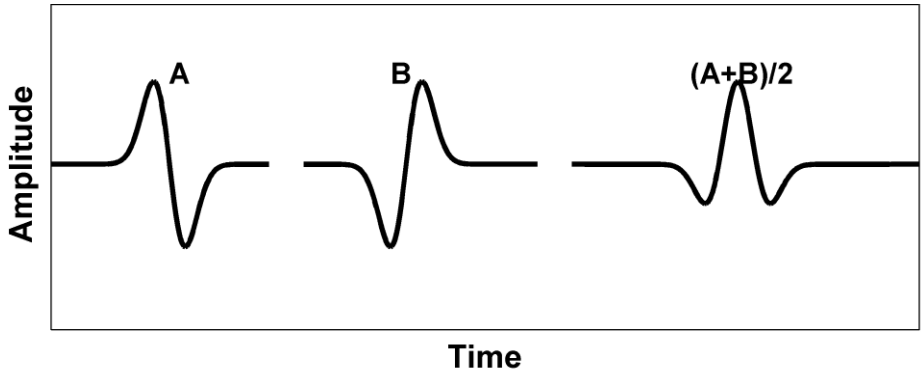

Fig. 17: Cartoon explaining the impact of averaging.

VI.F. Summary of Statistics Results

Before proceeding further, it is sensible to summarize what has been learned to this point.

1. The acoustic signal radiating to the low polar angles can be well represented by intermittent bursts of noise. In this study, these bursts are defined as regions of the signal with amplitudes larger than $1.5p_{RMS}$.
2. The fundamentally distinct nature of the low angle noise compared to sideline and upstream radiated noise is, once more, clearly revealed in this analysis. The primary conclusion is that the noise in the sideline and upstream directions does not have the distinctly intermittent nature. This conclusion should be tempered, however, by the fact that the analysis was limited by the sampling rate of the signal and it is therefore possible that noise events are present in the sideline and upstream angles but are very short-lived events.
3. Using a model with three important parameters in the acoustic signal (peak amplitude, event width, and the time between events), the following are now known.
    a. The distribution of peak amplitudes obeys a universal normal distribution across all polar angles and operating conditions once scaled by p_{RMS} of the original signal. The normal distribution (σ = 1.2) is close to the unit normal but slightly skewed toward larger amplitudes as already discussed.
    b. The distribution of event widths (looking only at the low polar angles) obeys a universal gamma distribution for all cases at a given polar angle once scaled by the mean event width ($\overline{\delta t}$). There are small variations in the gamma parameters with polar angle, but the

distributions are pretty well described by a single universal distribution for all angles below about ϕ = 50°. The fact that a gamma distribution accurately describes the event widths implies that the width of one event has no correlation to the width of other events – this result also implies that the noise sources are also independent.

c. The joint probability density functions of event width and amplitude show that there is a link between event amplitude and width that can be partially described by a simple geometric scaling.

d. The distribution of event intermittence has the same characteristics as the event width once scaled by the mean intermittence ($\overline{\Delta T}$). This implies that the occurrence of one event is not correlated to the occurrence of preceding or subsequent events. It is also found that the universal distribution that describes the event intermittence is the same as the distribution of the event width (gamma parameters $\ell \approx 6.0$ & $\xi = 0.17$).

e. There is a consistent relationship between the mean event width and the mean intermittence $\overline{\delta t}/\overline{\Delta T} = 0.128$. This implies some sort of link between the governing dynamics controlling these two quantities.

f. The mean event intermittence is a good predictor of the spectral peak frequencies for the low angles.

g. The directional dependence of the mean quantities interacts with the dependencies on diameter and temperature. These coupled dependencies make developing a scaling law for the data quite challenging.

4. Based on these observations, the entire signal for noise radiated to the low angles can be predicted in a statistical sense with knowledge of three quantities (p_{RMS}, $\overline{\delta t}$, and $\overline{\Delta T}$) along with the σ = 1.2 normal distribution and the gamma distribution ($\ell \approx 6.0$ & $\xi = 0.17$). It is actually possible to eliminate one or other of the mean quantities if the relationship in point 3.e ($\overline{\delta t}/\overline{\Delta T} = 0.128$) is used.

5. The mean width and intermittence are fairly insensitive to changes in the jet velocity in an unheated jet, but are significantly dependent on diameter and jet temperature. In the hot jet, there is also velocity dependence.

6. Directivity analysis of the mean quantities confirms the dependencies already discussed, but also shows that the polar angle dependence is intertwined with the diameter and temperature dependencies.

7. The averaged event waveform suggests that the typical instantaneous noise event consists of one positive and one negative swing of comparable amplitudes and widths, but not necessarily in that order.

Points 1 and 2 are consistent with the observations of Kœnig *et al.* [37]. Point 5 is also consistent with the work of Kœnig *et al.*, though their discussion utilizes an indirect inference from filtering in the wavelet domain as opposed to these event quantities. It is important to note that using the mean value of the distributions is a convenient scaling – it would work equally well to use the peak of the distribution or any other descriptive quantity of the distribution. If the appropriate shape is indeed one positive swing followed by one negative swing (or vice versa) of comparable amplitude, then the characteristic lifetime of that event would be two times the event widths discussed. Based on this analysis, the conceptual picture of the low angle jet noise signal appears as Fig. 18a.

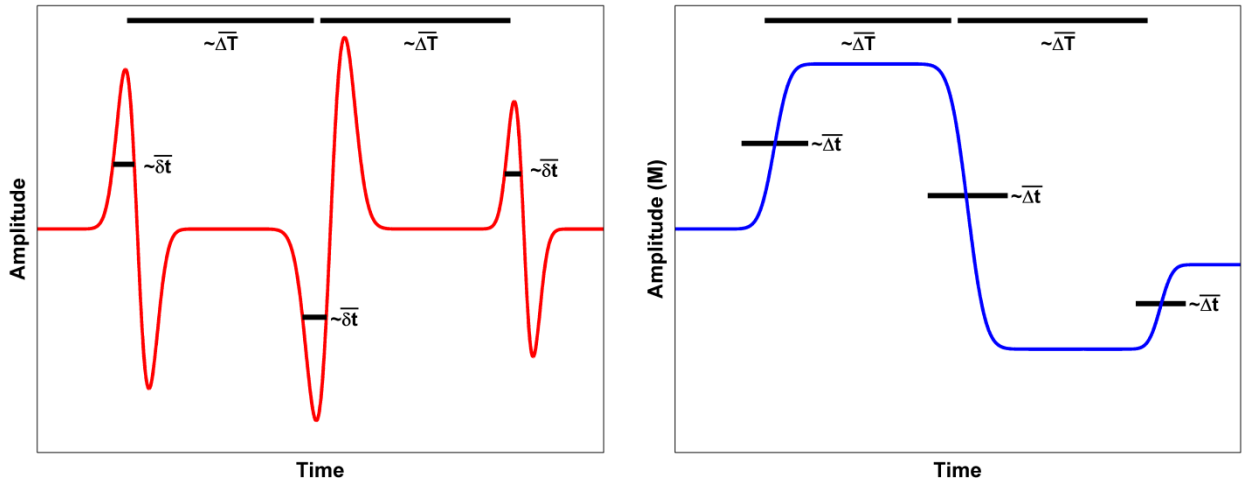

a) Far-field pressure fluctuations **b)** Integrated source fluctuations

Fig. 18: Cartoon of low angle jet noise signal based on the characteristics extracted from the analysis.

VII. Implications for Noise Sources

Using the picture of jet noise radiated to the low angles, the implications of this description on the noise sources are now discussed. The well-known solution to Lighthill's equation [1] for the acoustic pressure with the far-field approximation is

$$p(\underline{x},t) = \frac{x_i x_j}{4\pi |\underline{x}|^3 a_\infty^2} \frac{\partial^2}{\partial t^2} \int T_{ij} \left[\underline{y}, t - (|\underline{x}| - |\underline{y}| \cos\phi)/a_\infty \right] d^3\underline{y}. \tag{7.1}$$

Readers will note the evaluation of the source term T_{ij} at the retarded time—an essential feature of the solution. At a fixed radial distance, the evaluation in retarded time in the far-field is the same for all directions if the sources are acoustically compact (i.e. $|\underline{y}| \cos\phi$ may be neglected) so the spatial integral over the source volume can be written as

$$\int T_{ij} \left[\underline{y}, t - (|\underline{x}| - |\underline{y}| \cos\phi)/a_\infty \right] d^3\underline{y} = \Psi_{ij}(t), \tag{7.2}$$

where the source region has been evaluated at the retarded time. If the sources are not acoustically compact, Ψ_{ij} will have angular dependence – this possibility is briefly addressed at the end of this section. It has been shown that the essential feature of low angle jet noise is a fundamentally intermittent signal. Double integration in time of this signal implies that the components of the integrated source tensor (Ψ_{ij}) responsible for low angle noise are changing in time from one quasi-steady value to another. The second time derivative of this quasi-steady signal could produce the one-and-one signal proposed above. A cartoon showing the proposed behavior of Ψ_{ij} associated with the low angle noise cartoon is shown in Fig. 18b.

An example of such a source can be shown as follows – for simplicity, this initial derivation will be done for a single point in the far-field. A simple model for the one-and-one pulse is the first derivative of a Gaussian curve with an appropriate normalization. The noise event model (E) is a representation of the far-field pressure $p(\underline{x},t)$ at some fixed location for a small period of time:

$$E(t;T,\alpha,A) = A \frac{T-t}{\alpha} \exp\left[\frac{1}{2} - \frac{(t-T)^2}{2\alpha^2} \right]. \tag{7.3}$$

The noise event E has parameters governing its location in time (T), its duration in time (α) – i.e. width, and its amplitude (A). A positive value of A produces an event with the positive swing preceding the negative swing. This model has the following properties:

- The distance between the positive and negative peaks is 2α.
- Using the same adjacent isosceles triangle approximation of §VI.E gives a rough approximation of the FWHM (δt) of one half of the one-and-one pulse as α. In reality, the transcendental equation can be numerically solved to show that the FWHM = 1.60252α.

Integrating E twice in time produces the following

$$\int\int E(t;T,\alpha,A)dt\ dt = A\ \alpha^2\sqrt{\frac{e\ \pi}{2}}\mathrm{erf}\left[\frac{t-T}{\sqrt{2}\alpha}\right], \tag{7.4}$$

where erf is the error function and a constant offset is omitted for simplicity. In addition to supporting the previous argument, this result provides information about the behavior of the integrated source because

$$\int\int E(t;t_0,\alpha,A)dt\ dt = \frac{1}{4\pi|\underline{x}|a_\infty^2}\frac{x_i x_j}{|\underline{x}|^2}\Psi_{ij}, \tag{7.5}$$

for some fixed $\underline{x}$ remembering that Ψ_{ij} has been evaluated at the retarded time. The change in the magnitude (M) of the integrated source for a noise event at that particular location (i.e. $\frac{x_i x_j}{|\underline{x}|^2}\Psi_{ij}$) is then

$$M = 4\pi^{3/2}\sqrt{2e}A\ |\underline{x}|\alpha^2 a_\infty^2, \tag{7.6}$$

where an additional factor of two arises from the fact that the range of the error function is [-1,1]. The time interval over which this change in the integrated source occurs can be estimated as $\Delta t \approx 4\sqrt{2}\alpha$ from the known properties of the error function. Taking this back to the original definition of the event width (δt) as the FWHM of only one half of the one-and-one pulse, the time-scale of the change in the integrated source is $\Delta t \approx 3.53\delta t$. If typical values are inserted for the width (δt = 100 μs) and amplitude ($A = 1.75p_{RMS}$) for sound measured at ϕ = 30° and 100D from the jet where a_∞ = 340 m/s, then the typical amplitude and time-scale of the changes in the source field are $M = 4.09\ p_{RMS} D$ kg m^2 s^{-2} and Δt = 353 μs.

Bringing directivity into this picture, the first thing to note is that the far-field coordinate is an implicit variable in the parameters A, α, and T. The limitation of the present analysis is that it only allows for interpretation in two dimensions so the third dimension will not be discussed (i.e. x_1 is defined as the jet downstream axis and x_3 is discarded). This choice makes the discussion simpler and is not an unacceptable simplification. As has been discussed by many researchers previously [e.g. 45], the integrated source at some far-field coordinate takes on the form

$$\frac{x_i x_j}{|\underline{x}|^2}\Psi_{ij} = \cos^2\phi\,\Psi_{11} + \cos\phi\sin\phi\,(\Psi_{12}+\Psi_{21}) + \sin^2\phi\,\Psi_{22}. \tag{7.7}$$

This provides a map for ascribing the changes in the parameters of the typical noise event onto the components of the integrated source tensor (Ψ_{ij}). Evaluating the integrated source at $\phi \approx 0$, the combined information in §VI.D and (7.7) says that the dominant characteristic of Ψ_{11} should be the intermittent events. Ψ_{22} on the other hand (i.e. $\phi \approx \pi/2$) should behave much more like a white noise source. Looking at intermediate angles, the exact nature of the transition between the behavior of Ψ_{11} and Ψ_{22} is much more difficult to speculate on except to say that Ψ_{12} and Ψ_{21} must be contributing components that both decrease the width and increase the frequency of noise events in a fashion that limits to the behavior of Ψ_{22}. One obvious problem that arises in this interpretation is that the experimental results show that upstream angles do not recover the low angle intermittent behavior, contrary to the model prediction. This discrepancy can likely be accounted for by including source models not discussed in this simple analysis – e.g. non-compact source models such as those discussed by Cavalieri *et al.* [30] in which the components of the integrated source tensor have directivity.

While this result cannot directly point out the sources responsible for generating the noise events, it indicates the amplitude and temporal scales of the fluctuations in the flow-field that produce the noise events. Additionally, the intermittence information indicates how often these fluctuations occur. Armed with this information, future experiments and simulations can narrow their focus accordingly in the search for jet noise sources.

The most important result in terms of implications for existing noise source models is that there are essential dynamics missing from the current models. Currently, the best models for the low-angle jet noise are non-compact source models based on wave-packets [e.g. 30, 46]. As also discussed in §II.B, these wave-packet models typically model a noise source as consisting of a simple harmonic travelling wave and some sort of envelope function (often a Gaussian). The assumption that linear superposition is valid (for both the source field and the resulting acoustic field) is then used to create complexity in the acoustic field. While it may be mathematically possible to produce the rich behavior (described by the present statistical analysis) using this approach, the validity of linear superposition for the source field is tenuous. Furthermore, the rich behavior can only be accurately constructed by solving the

adjoint problem using a known acoustic field. A model that overtly contained the key features identified by statistical analysis would likely be a better physical description of the dynamics. While these wave-packet models show good agreement with the directivity patterns of the overall sound signal, they do not include (at least in any direction fashion) a number of the features revealed by statistical analysis. If the wave-packet model is discussed in terms of any one frequency, the following issues are observed:

1. Noise events are only quasi-periodic at best, but the wave-packet model predicts a purely periodic signal.
2. The event width and intermittence are correlated, but not in a way that would be well represented by the simple harmonic wave utilized in a wave-packet.
3. The event width and intermittence have directivity patterns that have no direct representation in the wave-packet model.

These weaknesses in the existing models should be examined to shed light on the best way to incorporate the essential dynamics revealed by statistical analysis.

VIII. Conclusions

Following on the previous works showing that jet noise has significant intermittent aspects, the present work hypothesized that these intermittent events are the dominant feature of jet noise. A definition and method of detection for noise events was devised and implemented. Using a large experimental database of acoustically subsonic jets with different velocities, diameters, and temperatures, these events were extracted from the noise signals. It was shown that a signal containing only these events retains all of the important aspects of the acoustic spectrum for jet noise radiating to shallow angles relative to the jet downstream axis. It is therefore concluded that these intermittent events are the essential feature of low angle jet noise.

The characteristics of these noise events were statistically analyzed. It was shown that these events are uncorrelated and that they can be statistically described in terms of three parameters (p_{RMS} of the original signal, the mean width of the events, and the mean time between events) and two universal statistical distribution curves. It was found that this intermittent nature occurred most prominently in the low angles and was not detectable for polar angles greater than about $\phi = 60°$. These parameters have strong dependencies on jet diameter and temperature. The parameters have a very weak dependence on jet velocity for unheated jets, but have significant velocity dependence in hot jets. The mean frequency of events was shown to be a good predictor of the spectral peak frequency. It was also found that there exists a strong correlation between the mean width and the mean intermittence. The ratio of these two quantities is consistently 0.128. This disagrees with the sinusoidal behavior of typical wave-packet models. The profile obtained by averaging all of the events indicates that the typical event may consist of one positive and one negative swing, but not necessarily in that order. A simple model for this kind of signal was used to derive a relationship between the characteristics of the noise events and the fluctuations in the integrated noise source volume. Finally, the relationship of the present analysis to existing wave-packet models was discussed. While the results found in this work cannot pinpoint noise sources, this new information should help narrow the focus of future work in the pursuit of understanding jet noise.

Acknowledgements

The support of this research by the NASA Glenn Research Center with Drs. James Bridges and Cliff Brown and the Air Force Office of Scientific Research with Dr. John Schmisseur is greatly appreciated. The authors also want to thank all of the AAPL personnel for providing the data for this project.

References

[1] Lighthill, M.J., "On Sound Generated Aerodynamically. I. General Theory", *Proc. Roy. Soc. London Ser. A* Vol. 211, No. 1107, 1952, pp. 564-587.

[2] Jordan, P., and Gervais, Y., "Subsonic jet aeroacoustics: associating experiment, modelling and simulation", *Exp. Fluids* Vol. 44, 2008, pp. 1-21.

[3] Tam, C.K.W., Golebiowski, M., and Seiner, J.M., "On the Two Components of Turbulent Mixing Noise from Supersonic Jets", AIAA Paper 1996-1716, 1996.

[4] Viswanathan, K., "Scaling Laws and a Method for Identifying Components of Jet Noise", *AIAA J.* Vol. 44, No. 10, 2006, pp. 2274-2285.

[5] Cabana, M., Fortuné, V., and Jordan, P., "Identifying the radiating core of Lighthill's source term", *Theor. & Comput. Fluid Dyn.*, 2007, pp. 20.
[6] Hileman, J., Thurow, B., Caraballo, E., and Samimy, M., "Large-scale structure evolution and sound emission in high-speed jets: real-time visualization with simultaneous acoustic measurements", *J. Fluid Mech.* Vol. 544, 2005, pp. 277–307.
[7] Viswanathan, K., "Analysis of the Two Similarity Components of Turbulent Mixing Noise", *AIAA J.* Vol. 40, No. 9, 2002, pp. 1735-1744.
[8] Panda, J., Seasholtz, R.G., and Elam, K.A., "Investigation of noise sources in high-speed jets via correlation measurements", *J. Fluid Mech.* Vol. 537, 2005, pp. 349-385.
[9] Bogey, C., and Bailly, C., "An analysis of the correlations between the turbulent flow and the sound pressure fields of subsonic jets", *J. Fluid Mech.* Vol. 583, 2007, pp. 71-97.
[10] Ukeiley, L., Tinney, C.E., Mann, R., and Glauser, M., "Spatial Correlations in a Transonic Jet", *AIAA J.* Vol. 45, No. 6, 2007, pp. 1357-1369.
[11] Hileman, J., Thurow, B., and Samimy, M., "Development and evaluation of a 3-D microphone array to locate individual acoustic sources in a high-speed jet", *J. Sound & Vib.* Vol. 276, No. 3-5, 2004, pp. 649-669.
[12] Ffowcs Williams, J.E., "Aeroacoustics", *Ann. Rev. Fluid Mech.* Vol. 9, 1977, pp. 447-468.
[13] Tam, C.K.W., "Jet Noise: Since 1952", *Theor. & Comput. Fluid Dyn.* Vol. 10, 1998, pp. 393–405.
[14] Crighton, D.G., "Jet Noise and the Effects of Jet Forcing", *Lecture Notes in Physics* Vol. 136, 1981, pp. 340-362.
[15] Crighton, D.G., "Acoustics as a Branch of Fluid Mechanics", *J. Fluid Mech.* Vol. 106, 1981, pp. 261-298.
[16] Powell, A., "Theory of Vortex Sound", *Journal of the Acoustical Society of America* Vol. 36, No. 1, 1964, pp. 177-195.
[17] Möhring, W., "On vortex sound at low Mach number", *J. Fluid Mech.* Vol. 85, No. 4, 1978, pp. 685-691.
[18] Kambe, T., and Minota, T., "Acoustic Wave Radiated by Head-On Collision of Two Vortex Rings", *Proc. Roy. Soc. London Ser. A* Vol. 386, 1983, pp. 277-308.
[19] Minota, T., and Kambe, T., "Observation of Acoustic Emission from Head-On Collision of Two Vortex Rings", *J. Sound & Vib.* Vol. 111, No. 1, 1986, pp. 51-59.
[20] Kambe, T., "Vortex sound with special reference to vortex rings: theory, computer simulations, and experiments", *Int. J. Aeroacoustics* Vol. 9, No. 1 & 2, 2010, pp. 51-89.
[21] Schram, C., Hirschbert, A., and Verzicco, R., "Sound Produced by Vortex Pairing: Prediction Based on Particle Image Velocimetry", *AIAA J.* Vol. 42, No. 11, 2004, pp. 2234-2244.
[22] Schram, C., Taubitz, S., Anthoine, J., and Hirschberg, A., "Theoretical/empirical prediction and measurement of the sound produced by vortex pairing in a low Mach number jet", *J. Sound & Vib.* Vol. 281, No. 1-2, 2005, pp. 171-187.
[23] Ran, H., and Colonius, T., "Numerical Simulation of the Sound Radiated from a Turbulent Vortex Ring", *Int. J. Aeroacoustics* Vol. 8, No. 4, 2009, pp. 317-336.
[24] Ko, N.W.M., Leung, R.C.K., and Tang, C.C.K., "The interaction of perturbed vortex rings and its sound generation. Part II", *J. Sound & Vib.* Vol. 228, No. 3, 1999, pp. 511-541.
[25] Fedorchenko, A.T., "On some fundamental flaws in present aeroacoustic theory", *J. Sound & Vib.* Vol. 232, No. 4, 2000, pp. 719-782.
[26] Obrist, D., "Directivity of Acoustic Emission from Wave Packets to the Far Field", *J. Fluid Mech.* Vol. 640, 2009, pp. 165-186.
[27] Kastner, J., Kim, J.-H., and Samimy, M., "A study of the correlation of large-scale structure dynamics and far-field radiated noise in an excited Mach 0.9 jet", *Int. J. Aeroacoustics* Vol. 8, No. 3, 2009, pp. 231–259.

[28] Grassucci, D., Camussi, R., Kerhervé, F., Jordan, P., and Grizzi, S., "Using Wavelet transforms and Linear Stochastic Estimation to study nearfield and turbulent velocity signatures in free jets", AIAA Paper 2010-3954, 2010.
[29] Cavalieri, A.V.G., Jordan, P., Gervais, Y., Wei, M., and Freund, J.B., "Intermittent sound generation and its control in a free-shear flow", *Phys. Fluids* Vol. 22, 2010, pp. 115113.
[30] Cavalieri, A.V.G., Jordan, P., Agarwal, A., and Gervais, Y., "Jittering wave-packet models for subsonic jet noise", *J. Sound & Vib.* Vol. 330, 2011, pp. 4474–4492.
[31] Kœnig, M. et al., "Farfield filtering and source imaging for the study of jet noise", AIAA Paper 2010-3779, 2010.
[32] Guj, G., Carley, M., Camussi, R., and Ragni, A., "Acoustic identification of coherent structures in a turbulent jet", *J. Sound & Vib.* Vol. 259, No. 5, 2003, pp. 1037-1065.
[33] Juve, D., Sunyach, M., and Comte-Bellot, G., "Intermittency of the Noise Emission in Subsonic Cold Jets", *J. Sound & Vib.* Vol. 71, No. 3, 1980, pp. 319-332.
[34] Low, K.R., Berger, Z.P., Lewalle, J., El-Hadidi, B., and Glauser, M.N., "Correlations and Wavelet Based Analysis of Near-Field and Far-Field Pressure of a Controlled High Speed Jet", AIAA Paper 2011-4020, 2011.
[35] Wei, M., and Freund, J.B., "A noise-controlled free shear flow", *J. Fluid Mech.* Vol. 546, 2005, pp. 123-152.
[36] Kastner, J., Samimy, M., Hileman, J., and Freund, J.B., "Comparison of Noise Mechanisms in High and Low Reynolds Number High-Speed Jets", *AIAA J.* Vol. 44, No. 10, 2006, pp. 2251-2258.
[37] Kœnig, M. et al., "Farfield filtering of subsonic jet noise: Mach and Temperature effects", AIAA Paper 2011-2926, 2011.
[38] Kœnig, M., Cavalieri, A.V.G., Jordan, P., and Gervais, Y., "Intermittency of the azimuthal components of the sound radiated by subsonic jets", AIAA Paper 2011-2746, 2011.
[39] Tanna, H.K., "An Experimental Study of Jet Noise. Part I. Turbulent Mixing Noise", *J. Sound & Vib.* Vol. 50, No. 3, 1977, pp. 405-428.
[40] Brown, C.A., and Bridges, J., "Small Hot Jet Acoustic Rig Validation", NASA-TR 2006-214234, 2006.
[41] Bridges, J., and Brown, C.A., "Validation of the Small Hot Jet Acoustic Rig for Jet Noise Research ", AIAA Paper 2005-2846, 2005.
[42] Cavalieri, A.V.G., Jordan, P., Gervais, Y., and Colonius, T., "Axisymmetric superdirectivity in subsonic jets", AIAA Paper 2011-2743, 2011.
[43] Kambe, T., "Influence of Viscosity on Aerodynamic Sound Emission in Free Space", *J. Sound & Vib.* Vol. 95, No. 3, 1984, pp. 351-360.
[44] Pope, S.B., *Turbulent Flows*: Cambridge University Press, 2000.
[45] Crighton, D.G., "Basic Principles of Aerodynamic Noise Generation", *Prog. Aerosp. Sci.* Vol. 16, No. 1, 1975, pp. 31-96.
[46] Papamoschou, D., "Wavepacket Modeling of the Jet Noise Source", AIAA Paper 2011-2835, 2011.